

Investigation of Metal Organic Frameworks for seasonal thermal energy storage

A comparison of a number of MOFs on energy storage density

Marco Leenders

Delft University of Technology



Photo: Boiler heated by adsorption driven heat pump using zeolites, in tandem with a gas heater and environmental heat (produced by Viessmann Werke GmbH & Co KG)

Investigation of Metal Organic Frameworks for seasonal thermal energy storage

A comparison of a number of MOFs on energy storage density

By

Marco Leenders

in partial fulfilment of the requirements for the degree of

Master of Science
in Applied Physics

at the Delft University of Technology,
to be defended publicly on August 21st 2017, at 15.00 PM

Supervisor:	Prof. dr. F. Kapteijn
Thesis committee:	Prof. dr. F. Kapteijn Dr. Ir. A Schmidt-Ott Dr. Ir. M. Makkee

An electronic version of this thesis is available at <http://repository.tudelft.nl/>.



Abstract

Formed from an organic linker and a metal salt cluster, Metal Organic Frameworks (MOFs) are highly crystalline materials with a large surface area, pore size and pore volume. Some of these MOFs show a step-wise water adsorption behaviour. This would make them suitable for seasonal thermal heat storage through water adsorption, due to their high stability in a moist air environment and a relatively large adsorption capacity.

This thesis is dedicated to modelling MIL-101(Cr), MIL-100(Fe), Aluminium fumarate, MOF-841(Zr), CAU-10(Al)-H, MIL-125(Ti)-NH₂, MIL-160(Al) and CPO-27(Ni). The adsorption capacity was tested using two situations with a different set of temperatures. From these MOFs, three of the better performing MOFs were eventually tested, to measure the water adsorption energy density. With this data, the expected needed storage volume of the MOF was estimated, where the best MOF was chosen.

*“Nature conceals her secrets because she is sublime,
not because she is a trickster”*

- Albert Einstein, world-renowned theoretical physicist

Preface

This is the report of a master's thesis, a study which is part regarding seasonal thermal energy storage, using water vapour adsorption. This study was based on a number of relatively well-known Metal Organic Frameworks (MOFs). This thesis report has been written to fulfil the graduation requirements of the master Sustainable Energy Technologies at the Delft University of Technology (TU Delft), as a joint project between the Delft University of Technology and the institute Toegepast Natuurwetenschappelijk Onderzoek (TNO). I was engaged in studying these MOFs from October 2016 to June 2017.

I would like to thank my supervisors from both TU Delft: Prof. Dr. Freek Kapteijn and Martijn de Lange; and from TNO: Ruud Cuypers and Ard-jan de Jong for their guidance and support during my study. I would also like to thank Alexey Pustovarenko for aiding me with the first synthesis of the MOFs and providing me with training for the characterization of the MOFs, Willy Rook for helping me perform the water and nitrogen adsorption analyses, Aletta Kaas for helping me with the water adsorption measurements at TNO and Joris Salari for allowing and helping me with the DSC/TGA measurements at TNO. I would also like to thank the colleagues of Catalysis Engineering for the positive atmosphere, which helped me to stay motivated, but last yet foremost, I would like to thank my parents for their support and guidance when needed.

M. Leenders

Delft, June 2017

List of abbreviations

P_o	saturaion pressure of the adsorbent (water or nitrogen)
w	water asorption density, as expressen in volume of liquid water equivalent (at 25°C) over the volume of the MOF
ρ_i	density of substance i
A	adsorption potential (in kJ/mol)
λ	wavelength of light (in nm)
T_{des}	desorption temperature (operating temperature of the would-be solar heat panel)
T_{ads}	temperature of water adsorption
T_{ev}	operating temperature of the evaporator
T_{cond}	operating temperature of the condenser

Contents

1	Introduction and modelling	8
1.1.	Introduction to seasonal thermal energy storage	8
1.2.	Overview of the thesis	11
2	Modelling	12
2.1.	Equations used in modeling	12
2.2.	Modelling conditions	13
2.3.	Model results and choosing the MOFs for further study	13
3	Synthesis	15
3.1.	CAU-10(Al), introduction and synthesis	15
3.2.	MIL-160(Al), introduction and synthesis	16
3.3.	CPO-27(Ni), introduction and synthesis	17
4	Characterisation	19
4.1.	Characterization of CAU-10(Al)	19
4.2.	Characterization MIL-160(Al)	23
4.3.	Characterization of CPO-27(Ni)	26
5	Activation of the MOFs and adsorption	29
5.1.	CAU-10(Ni)-H	29
5.2.	MIL-160(Al)	34
5.3.	CPO-27(Ni)	39
6	Energy density	43
6.1.	CAU-10(Al)	43
6.2.	MIL-160(Al)	44
6.3.	CPO-27(Ni)	45
6.4.	Calculation of the needed storage volume	45
7	Production of the organic linkers	46
7.1.	Isophthalic acid (CAU-10(Al))	46
7.2.	Furandicarboxylic acid (MIL-160(Al))	46
7.3.	2,5-dihydroxyterephthalic acid (CPO-27(Ni))	46
8	Discussion	47
9	Conclusion	48
	Bibliography	49
	Appendix	51
A.2	Synthesis tables	51
A.2	infrared spectroscopy of the third batch of CAU-10(Al) samples	52
A.3	water adsorption of the first sample of MIL-160(Al)	53
A.4	water adsorption of the second sample of MIL-160(Al)	56
A.5	Temperature profile used for the STA measurements	59
A.6	TGA profile of CAU-10(Al) used for the STA measurements	60
A.7	TGA profile of MIL-160(Al) used for the STA measurements	61
A.8	TGA profile of CPO-27(Ni) used for the STA measurements	62

1

Introduction and modelling

1.1. Introduction to seasonal thermal energy storage

Given the predicted increase in this energy consumption, the need to convert from conventional power sources to more sustainable forms of energy production seems to become increasingly apparent. About a third of the global energy production is consumed by households. Most of this energy goes into heating of houses.^[1]

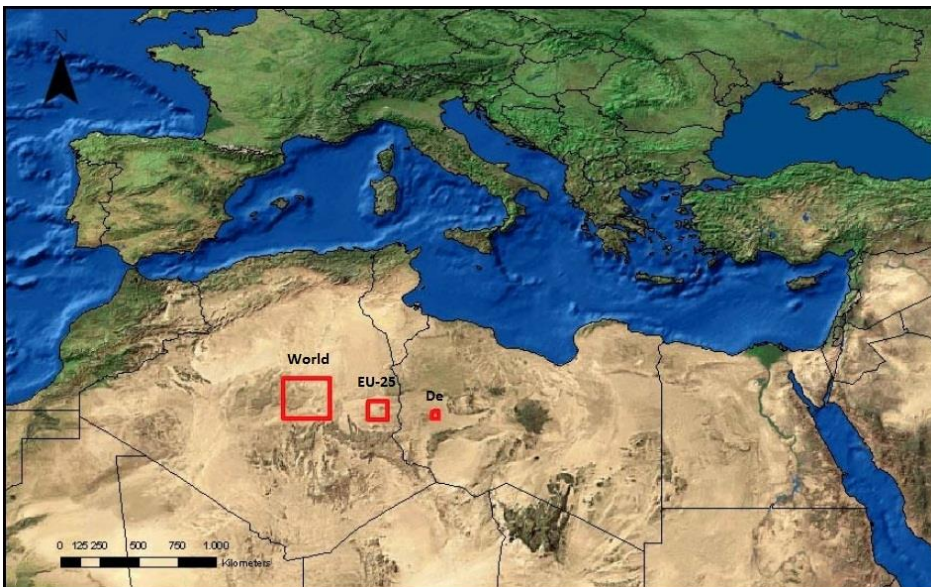


Figure 1 area needed to cover the electricity demand for the world, the EU-25 and Germany, respectively. Based on the average local electrical yield of PV's and 2005's global energy demand^[2]

With the vast amounts of sunlight and the area needed for energy production is relatively low (as seen in **Figure 1**), it can then be seen that sunlight is the source with the most potential. Storage however becomes a challenge, since the moments with the highest heat demand usually are the moments with the least sunshine. Therefore, thermal energy storage is crucial to compensate the moments of energy production shortage and surplus. This also includes seasonal thermal energy storage, i.e. the energy surplus in summer as opposed to the winter's energy shortage (as seen in **Figure 2**).

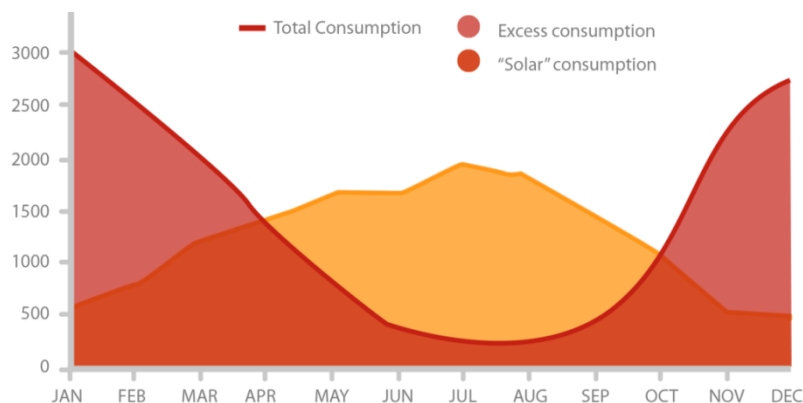


Figure 2 Annual energy consumption (red) and (normalised) production (yellow)^[3]

This poses a challenge when using some energy storage methods, since energy loss over time should be kept at a minimum. When this method is used in households, one must also take into account the safety of the system in case of failures. The methods of long-term energy storage designed for households include, but are not limited to:

Underground Seasonal Thermal Energy Storage (STES) is commonly used in large buildings and greenhouses, because of the underground's large capacity of heat^[4].

Generating electrical energy, where this electrical energy can then be stored into a fuel using fuel cells or in charged batteries. When thermal energy is needed, an electrical heater can be used.

Energy can be stored in the form of potential energy or kinetic energy, e.g. dams or using a flywheel

Produced energy can be stored in the form of pressurized gas, which can be stored underground^[5].

Energy can also be stored through chemisorption. In this, water is the mostly used adsorption liquid, while the absorption material is usually a salt hydrate or a metal oxide (reacting to hydroxide)^[6]

	potential advantages	challenges
STES	<ul style="list-style-type: none"> + sometimes high storage capacities available + relatively maured technology 	<ul style="list-style-type: none"> - not everywhere possible - set-up is expensive - not decentralised
pressurized gas	<ul style="list-style-type: none"> + versatile: gas tanks an be stored anywhere + relatively matured technology 	<ul style="list-style-type: none"> - low efficiency of compressors - equipment failure potentially hazardous - low volumetric/mass energy density
electrical	<ul style="list-style-type: none"> + versatile: fuel cell fuel can be stored anywhere + matured technology 	<ul style="list-style-type: none"> - low efficiency of PV panels - structural integrity of the batteries / fuel cells - Fuel storage
zeolites	<ul style="list-style-type: none"> + high stability achievable 	<ul style="list-style-type: none"> - low storage capacity - slow heat transport - desorption temperatures are very high
salt hydrates	<ul style="list-style-type: none"> + well-known salts available (e.g. NaS or CH₃COOH) + high storage capacity 	<ul style="list-style-type: none"> - slow heat transport - possible stability issues due to dissolving of the salt
hydroxides	<ul style="list-style-type: none"> + well-known salts available (e.g. NaOH or KOH) + high energy storage capacity 	<ul style="list-style-type: none"> - slow heat transport - possible stability issues due to issolving of the salt
silica gel	<ul style="list-style-type: none"> + well-known high stability 	<ul style="list-style-type: none"> - low capacity

Table 1 overview of advantages and disadvantages of several thermal storage methods, with the pros and cons for each

Because the water can be stored in a liquid form in a separate tank, this makes for a very viable way of storing heat energy for long periods of time, making it a viable option for seasonal heat storage.

Although stable materials can be used for physisorption, finding the right material with a high enough energy density proves challenging. The most common chemical used to adsorb is water vapour, due to its non-toxicity and high condensation enthalpy. Common adsorbing materials are silica gel and zeolites. The physisorption of water vapour releases energy in the form of heat, which is fed to the system when the water evaporates out of the absorber.

Another adsorbing material that can be used is MOFs. When an organic ligand has multiple complex binding positions, these can combine with the metal oxide, arranging such, that a 1D, 2D or 3D framework can be formed. Such Metal Organic Frameworks (MOFs) have pores that can adsorb small molecule substances, such as water. Because there's a variety of substances and complexing metals, this enables one to choose among a wide variety of different MOFs. Because activated MOFs work based on physisorption, mass and thermal transport is a lot faster than most chemisorption based materials, while its adsorption capacity is still significant. The proposed setup for a household is depicted in **Figure 3**. During the summer (solar heat abundance), The solar heat panel will heat the heat carrying liquid. This carrying liquid will in turn flow to a heat exchanger, heating a storage tank with the Metal Organic Framework in an environment with water vapour. During this surplus, the water is desorbed from the MOF, cooling down the pipe that's going through the house, which can then be used for cooling the household. During a shortage, the desorbed water can then be adsorbed into the MOF, providing heating for the house. To decrease the volume needed for the storage of the water, the liquid is condensed and evaporated whenever needed.

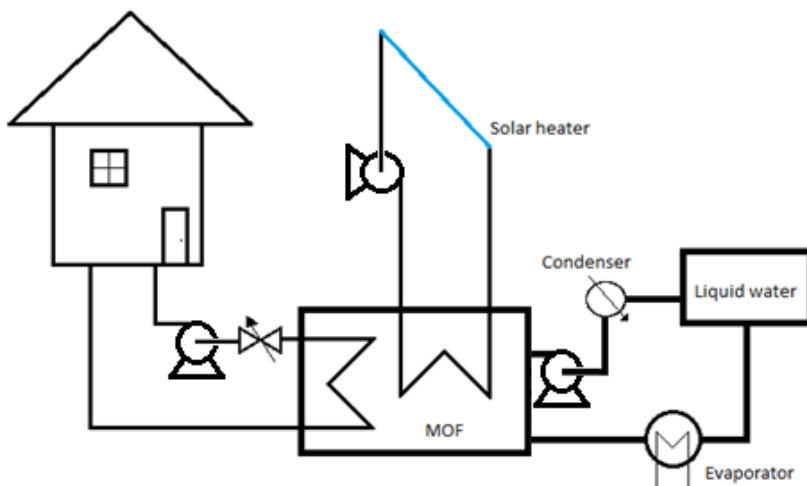


Figure 3 Schematic sketch of a household using MOFs to store seasonal heat. During an energy surplus, the water from the MOF evaporates and is condensed, providing cooling. During shortage, the liquid water is evaporated and adsorbed back into the MOF.

The temperatures used for these steps are as follows: Desorption temperature should be around 90°C, for the solar heater to be effective, evaporator temperature was chosen to be around 10-20°C, to be effective in winter without excessive heating, adsorption temperature should be around 40-60°C. 40°C would be more suited for household heating, while 60°C is more suited for hot water production, since 55°C is the minimum temperature for hot water and a temperature difference of around 5°C .

$$T_{\text{des}} = 90^{\circ}\text{C}$$

$$T_{\text{ev}} = 10\text{-}20^{\circ}\text{C}$$

$$T_{\text{ads}} = 40\text{-}60^{\circ}\text{C}$$

$$T_{\text{cond}} = 20\text{-}30^{\circ}\text{C}$$

Using these conditions, a number of MOFs were chosen based on For the MOF to be effective, the water adsorption must be high enough to be effective at these temperatures. Eight of the most common MOFs have been modelled, of which the most promising choices were tested.

1.2. Overview of the thesis

For this thesis, a model was initially used to select a few of the interesting MOFs, from the equations that were used to calculate the water adsorption from adsorption isotherms found in the literature. Three promising MOFs were chosen from this for further study.

These three MOFs are, after synthesis, first characterised using X-Ray Diffraction (XRD) spectroscopy to test the crystal structure and compare this to the given value, InfraRed (IR) spectroscopy was used to measure any larger amount of amorphous impurities. Scanning Electron Microscopy (SEM) was then used to detect the shape of the crystals and to estimate the crystal size. A ThermoGravimetric Analysis (TGA) is then used to spot impurities and compare the ash content with the expected values, but a TGA can also show the adsorption capacity of the MOF.

To measure the adsorption capacity, a nitrogen sorption analysis was first performed to test the activity of the MOF, which is then followed by a water adsorption analyser, where the pressure was varied under a constant temperature. This would yield an adsorption isotherm with the water adsorption measured over the water vapour pressure. Activation was done in a vacuum oven overnight. It was chosen to have the synthesis/characterisation and activation/adsorption sections split into two chapters for a clearer construction of the report.

The energy density of the MOF during adsorption and desorption was measured using a Simultaneous Thermal Analyser (STA), which can be described as a combination of a differential scanning calorimeter and a TGA. This will measure the heat flow over measured time, where integrating over the full adsorption would yield the energy of adsorption and desorption.

It was chosen to have the experimental and results sections in this this report discuss the data in separate chapters: synthesis, characterisation, adsorption (both nitrogen and water) and energy density, in the respective order. This is because it is thought that this order will provide the best overview of this work.

From the energy density data, an expected needed storage volume will be deducted based on the average heat consumption of a Dutch household. This will then be followed by a short qualitative analysis (literature study) on the production of the MOF's linker. From all of the data gathered, plus the brief analysis on linker production, the best performing MOF will be chosen, which will answer the main question of this thesis.

2

Modelling

2.1. Equations used in modeling

For the system proposed, it was assumed that the heat coming from the solar heat panel is 90°C, since this is assumed to be an effective temperature for the heating fluid in a solar heat panel. To have this setup operate at optimal conditions, the setup should be able to run at various temperatures. Having a desorption temperature that is too high would decrease the efficiency of the solar heat panels too much. Since it was assumed that water is used for the heat carrier fluid of the panel, the operating initial temperature of desorption was assumed to be around 90°C for the model (a bit lower than the boiling temperature of water at $P = 1$ atm). The condensation temperature of the water basin is assumed to be between 20-30°C, since this temperature should not be too different from the outside temperature.

During winter, the evaporation temperature of the basin was assumed to be between 10-20°C. Although the outside temperature during winters can be significantly lower in the Netherlands, the temperature is still chosen, because some water heating is permitted to increase the adsorption efficiency. For adsorption, the temperature to be used was set between 40-60°C, since 40°C could be a suitable temperature of the circulating water for household heating, while water heating for use of hot water, this is not sufficient, since water at this temperature is suitable for household (consumable) water needs.

The adsorption capacity is dependent on both the (partial) water vapour pressure and the temperature. For this, the adsorption potential from Goldman and Polanyi^[7] will be introduced as A and a working factor W , which are defined as follows:

$$A \equiv RT \ln \left(\frac{p_{sat}(T)}{p} \right) \quad (1)$$

$$W \equiv \frac{q(T,p)}{\rho_{liq}(T)} \quad (2)$$

Plotting the working factor over the adsorption potential reduces the amount of free variables to one. This makes modelling the MOFs significantly easier, since the adsorption is now a function of $f(A)$, instead of $f(p,T)$.

In order to model this, the difference in working factor ΔW should be as high as possible, since a higher water adsorption would lead to a higher energy density. This is done by altering the adsorption potential such, by changing the temperature and/or pressure of the system. The two relevant potentials will hereby be referred to as the adsorption potential A_{ads} and desorption potential A_{des} . These are equal to:

$$A_{ads} \equiv RT_{ads} \ln \left(\frac{p_{sat}(T_{ads})}{p_{sat}(T_{evap})} \right) \quad (3)$$

$$A_{des} \equiv RT_{des} \ln \left(\frac{p_{sat}(T_{des})}{p_{sat}(T_{cond})} \right) \quad (4)$$

2.2. Modelling conditions

With the chosen temperature requirements, two initial cases have been chosen hereby referred to as Case 1 and Case 2. In Case 1, the lowest temperature of evaporation and condenser, but the highest possible temperature of adsorption were chosen. This was to view the performance at the conditions of the highest temperature difference, which would give in turn a higher value for $P_{\text{sat}}(T_{\text{ads}}) / P_{\text{sat}}(T_{\text{evap}})$, while giving a lower value for $P_{\text{sat}}(T_{\text{des}}) / P_{\text{sat}}(T_{\text{cond}})$. This in turn will decrease the difference between A_{ads} and A_{des} , giving less favourable values, thermodynamically speaking. This case would be suitable for the production of hot water.

Case 2 was set to have the highest temperature of evaporation and condenser, but the lowest possible adsorption temperature. This will result in a lower value for $P_{\text{sat}}(T_{\text{ads}}) / P_{\text{sat}}(T_{\text{evap}})$, while giving a higher value for $P_{\text{sat}}(T_{\text{des}}) / P_{\text{sat}}(T_{\text{cond}})$. This will thereby decrease the difference in adsorption and desorption potential, making the case more favourable, thermodynamically, but with only the ability to use the water for household heating and no for any hot water production.

Calculating the adsorption and desorption potential in these two cases, two values of A can be obtained per case. **Table 2** provides an overview of the temperatures used, with the calculated adsorption potentials.

condition	T (°C)	
	case 1	case 2
evaporation	10	20
condenser	20	30
adsorption	60	40
desorption	90	90
A_{ads}	7,6	2,9
A_{des}	10,3	8,5

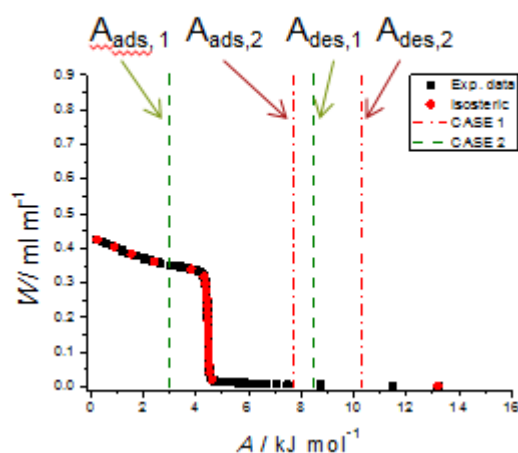
Table 2 Operation temperatures chosen in two cases with the calculated adsorption potentials, which can be used for modelling

From this, it can be concluded that being able to operate with smaller differences in adsorption potentials (between adsorption and desorption) would lead to more favourable conditions for the system. Given that the MOFs require high differences in W to have a sufficient storage capacity, a steep (preferably step-wise) $W(A)$ curve required to be efficient.

2.3. Model results and choosing the MOFs for further study

The MOFs chosen to be modelled were not only chosen because of their steep $W(A)$ curve, but also for their high stability in an aqueous environment, with a water adsorption isotherm at at least two temperatures available to verify the reliability of the model. Based on these requirements, 8 different MOFs were chosen: MIL-101(Cr), MIL-100(Fe), Aluminium fumarate, MOF-841(Zr), CAU-10(Al)-H, MIL-125(Ti)-NH₂, MIL-160(Al), MOF-801(Zr) and CPO-27(Ni). Using these conditions, the performance was modelled using the two cases presented. **Graph 1** shows the $W(A)$ plot of CAU-10(Al), with the calculated values for A seen as dotted lines (red = case 1; green = case 2).

Example: CAU-10(Al)



Graph 1 W(A) plot of CAU-10, with the values for A from the two cases, set as an illustrative example how the MOFs were modelled

From this example plot of CAU-10(Al)-H, it can be seen that the difference ΔW is nearly 0 in case 1 (hot water production), but ΔW is significantly larger at case 2 (house heating). This is due to the very steep incline. This means CAU-10(Al)-H is a suitable sample to be tested for case one, though it seems unsuitable for use of hot water production.

Using this method and applying these to all cases, the ΔW can be calculated, as are being depicted in **Table 3** depicts the calculated values.

MOF	ΔW , case 1 (mL/mL)	ΔW , case 2 (mL/mL)
MIL-101(Cr)	0,01	0,06
MIL-100(Fe)	0,02	0,24
Al-fumarate	≈ 0	0,25
MOF-841(Zr)	≈ 0	0,48
CAU-10(Al)-H	≈ 0	0,35
MIL-125(Ti)-NH ₂	0,01	0,26
MIL-160(Al)	0,04	0,36
CPO-27(Ni)	0,16	0,21

Table 3 Modelled values for the MOFs initially chosen, bold numbers represent significant adsorption capacities

From this, it's visible that suitable MOFs are MOF-841(Zr), CAU-10(Al)-H, MIL-160(Al), MOF-801(Zr) and CPO-27(Ni) are suitable MOFs to be tested.

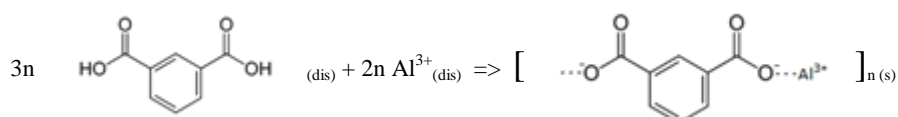
From the list depicted in **Table 3**, MOF-841(Zr) was excluded due to its difficulty to produce the MOF (the linker that was not available commercially), leaving with CAU-10(Al)-H and MIL-160(Al) for case 2 and CPO-27(Ni) for case 1 as the MOFs with the most potential. All three MOFs were tested on both cases in this thesis.

3

Synthesis and characterization

3.1. CAU-10(Al), introduction and synthesis

CAU-10(Al)-H is a Metal Organic Framework (MOF) that is shown to have water adsorbing effects, due to its hydrophilic pores. It is synthesized from Aluminium sulphate and isophtalic acid using a DMF/water mixture as solvent. The reaction takes place under an elevated temperature and pressure (135°C in an autoclave).



The resulting aluminium isophtalate hydroxide ($\text{Al}(\text{C}_8\text{O}_4\text{H}_4)\text{OH}$) is then cleaned by means of centrifuging using DMF as its liquid. **Figure 4** Depicts a schematic of the structure of CAU-10(Al)-H.

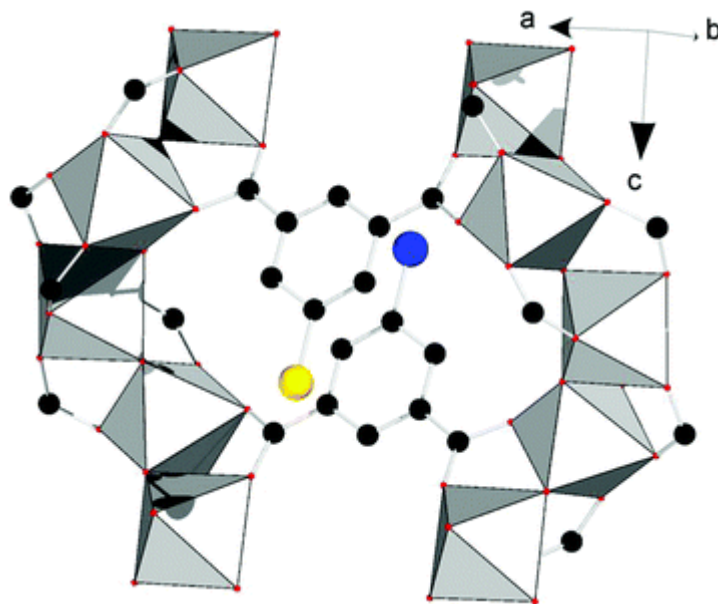


Figure 4 schematic of the structure of CAU-10. The octahedrons represent the aluminium structure, while the black dots represent the carbon atoms of the organic isophtalate linker. The blue and yellow circles represent hydrogen atoms in the case of CAU-10(Al)-H.^[8]

The synthesis of CAU-10(Al)-H was based on the publication of de Lange et al.^[9] performed from isophtalic acid as linker and aluminium sulphate as its aluminium source. The aluminium sulphate is dissolved in deminwater, while isophtalic acid (due to the low solubility in water) was dissolved in DMF. The details of the synthesis are as follows: 0,16 grams of isophtalic acid was dissolved in 0,76 grams of DMF 0,64 grams of aluminium sulphate octadecahydrate is dissolved in 3,3 mL deminwater.

To see if it was needed to dissolve the two solutions before mixing, initially two synthesis pathways in parallel were carried out: one sample was made by mixing all components into one autoclave, while in the other sample, the two mixtures were dissolved before mixing the two in an autoclave.

Both mixtures were placed in a 15 mL autoclave, to then be placed in an oven at 135°C overnight. The solid powder was separated from the liquid using a centrifuge at 6000 rpm for 20 minutes. The liquid phase was then decanted as much as possible.

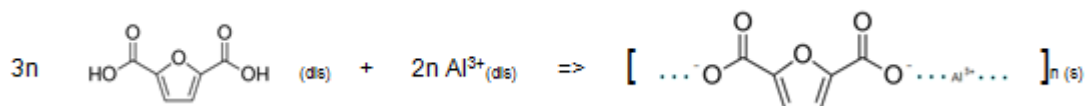
From these samples, the X-ray diffraction was measured using a Bruker Advance D8, along with powder infrared absorption and scanning electron microscopy to see if the two different ways of synthesizing would have different results as regards to the end product. A thermographic analysis was performed to quantify the amounts of impurities, such as loose linker, ash content or adsorbed solvents.

Activation is performed stirring ethanol at a temperature of 80°C overnight, followed by placing it in a vacuum oven at 150°C overnight. Storing was done in a desiccator at a pressure of 1 mbar, transportation was performed by placing the sample vial in a nitrogen glove box, where the sample holder was placed in a bigger (plastic) sample holder to create a small, water-free environment, suitable for transportation.

Table S - 1 shows the masses used for all the CAU-10(Al) samples synthesized, with a yield calculation for every synthesis, based on the amount of moles of bound linker divided by the amount of added linker

3.2. MIL-160(Al), introduction and synthesis

MIL-160(Al) is a Metal Organic Framework (MOF) that is shown to have water adsorbing effects, due to its hydrophilic pores. It is synthesized from aluminium chloride and 2,5-furandicarboxylic acid (from now on referred to as fdcaH₂ for pragmatic reasons, whereas the conjugated base will be referred to as fdca²⁻ for the same reason), using water as solvent (with small amounts of sodium hydroxide added to increase the solubility of the acid). The reaction takes place under atmospheric temperature and at a temperature of 110°C in a reflux:



The resulting aluminium furandicarboxylate hydroxide (Al(C₇O₅H₂)OH) is then cleaned by means of centrifuging using water as the liquid, using ethanol as cleaning to remove the remaining water. Activation is then performed using ethanol at a temperature of 80°C, followed by placing in a vacuum oven at 150°C.

Figure 5 Depicts a schematic of the structure of MIL-160(Al).

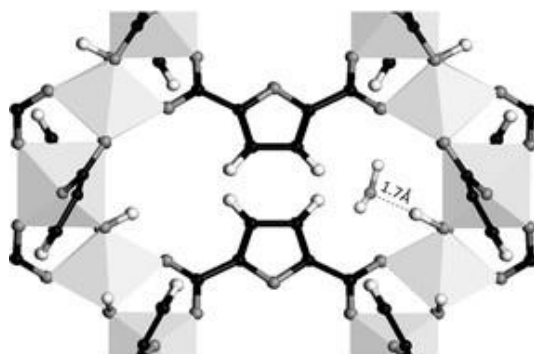


Figure 5 schematic of the structure of MIL-160(Al). The tetrahedrons represent the aluminium oxide groups, while the black shape represents the furandicarboxylate linker (the pentagon represents the furan group, while the neighbouring Y-shapes bound to the aluminium represent the carboxylate. The white dots represent the hydrogen atoms.

The synthesis of MIL-160(Al) was initially based on the work of Cadieau et al.^[10] MIL-160(Al) was initially synthesized by pouring 60 mL of deminwater into a 100 mL glass beaker. 1,1729 g of furandicarboxylic acid and 0,2557 g of sodium hydroxide (to increase the solubility of the carboxylic acid) was dispersed in about 20 mL from the beaker, while 1,8062 g of aluminium chloride was dissolved in the remainder of the water.

Both mixtures were added in a 250 mL round bottom flask, which seemed to partially dissolve the white powder upon mixing. The mixture was then heated to 100°C using an oil bath. This was left to stir overnight. After that was done, the solid was separated from the liquid using a centrifuge set at 6000 rpm for 20 minutes. The liquid was then decanted from the solid before being washed with clean water, where the solid was dispersed and centrifuged at 6000 rpm for 20 minutes again. The liquid phase was decanted afterwards and the cycle was repeated once more. This was then followed by washing with clean ethanol once, where the suspension was dispersed and centrifuged at 6000 rpm for 20 minutes again. The liquid phase was decanted for as much as possible, and the remaining paste was placed in a drying oven at 80°C overnight. The weight of the resulting powder was 0,4496 g. When the adsorbed content of water is known, one can then calculate the yield of the synthesis.

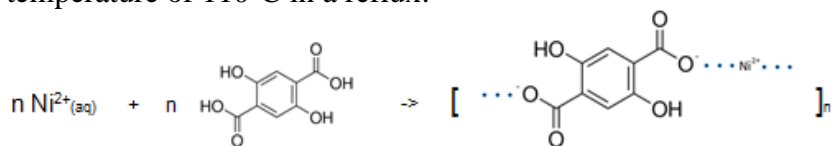
From this powder, SEM images were taken to see the resulting crystals. X-ray diffraction was used to measure the crystallinity and quantify the crystallite size. Infrared spectroscopy was used to measure the vibrations of the functional groups, which can be used to qualitatively measure the presence of any impurities, such as adsorbed water or any unbound linker. A Thermographic Analysis was performed to quantify these impurities further.

The cleaning of the material was one by dispersing the MOF in 150 mL ethanol and heating the suspension to 70°C, leaving this overnight. Afterwards, the suspension was partially poured into a 50 mL centrifuge tube, where the two phases were separated using a centrifuge at 6000 rpm for 10 minutes, decanting the liquid. More of the suspension was added and centrifuged, followed by decanting again. This was repeated until all of the solid was out of the flask (including rinsing with ethanol to ensure all of the powder was poured in the flask. After all was placed in the centrifuged, the solid was dispersed in clean ethanol, and centrifuged again at 6000 rpm for 10 minutes, followed by decanting the liquid phase again. This was repeated once more, followed by placing the remaining white paste in a vacuum oven at 150°C overnight. This was then immediately transferred to a glove box (N₂, overpressure around 10 mbar, [H₂O] ≈ 1-10 ppm), where it was packaged in a glass bottle, which was in turn packaged in a polypropylene bottle, both with a screw cap. This was then kept inside the glove box for storage until the next measurement, where the doubly-packaged MIL-160(Al) was transferred before opening. Every time after the package has been opened, the sample was activated again in the vacuum oven.

Table S - 2 shows the masses used for all the MIL-160(Al) samples synthesized, with a yield calculation for every synthesis, based on the amount of moles of bound linker divided by the amount of added linker.

3.3. CPO-27(Ni), introduction and synthesis

CPO-27(Ni) is a Metal Organic Framework (MOF) that is shown to have water adsorbing effects, due to its hydrophilic pores. It is synthesized from aluminium chloride and 2,5-dihydroxyterephthalic acid (from now on referred to as dhtpH₂ for pragmatic reasons, whereas the conjugated base will be referred to as dhtp²⁻ for the same reason), using water as solvent. The reaction takes place under atmospheric temperature and at a temperature of 110°C in a reflux:



The resulting nickel dhtp²⁻ hydroxide (Ni(C₈O₄H₄)) is then cleaned by means of centrifuging using water as the liquid, using ethanol as cleaning to remove the remaining water. **Figure 6** depicts a schematic of the structure of CPO-27(Ni).

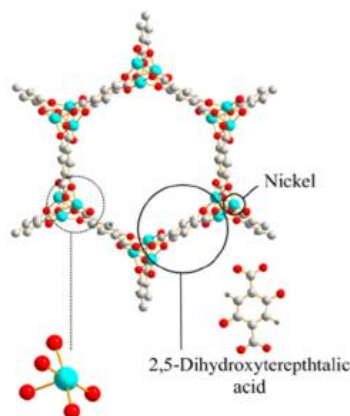


Figure 6 Schematic of the structure of CPO-27(Ni). The blue and red dots represent the nickel and the oxide, respectively. The grey groups of grey dots on each face of the hexagon represent the 2,5-dihydroxyterephthalate linker

The synthesis of CPO-27(Ni) was based on the work of Cadot et al.^[10]. The CPO-27(Ni) (MOF-74(Ni)) samples were synthesized by dissolving 1,2538 g of Nickel acetate tetrahydrate in 50 mL of water. Another solution was prepared using 50 mL of water and 0,4975 g of 2,5-dihydroxyterephthalic acid. Both are mixed for 10-15 minutes, where the nickel was dissolved into a green liquid, but the dihydroxyterephthalic acid was still a suspension of a yellow powder in a yellow liquid. The two solutions were then added together in a 250 mL round-bottom flask, where the resultant mixture was a dark-green, clear mixture. The mixture was placed in a reflux at 110°C, using an oil bath. After approximately one hour, the content of the flask seemed to turn into a yellow suspension. The reaction was left to run for two more hours before the setup was allowed to cool to room temperature.

Washing was performed by centrifuging at 6000 rpm, using water as rinsing material, decanting the liquid every time. This was repeated twice, followed by using ethanol with a centrifuge once more. After decanting the ethanol liquid, the remaining paste was placed in an 80°C drying oven overnight. The powder was then placed in a small glass sample holder.

The crystalline structure was measured using X-ray Diffraction, the chemical structure was characterised using powder Infrared spectroscopy, while scanning electron microscopy was used to see the crystal structures and their shapes and sizes. A thermographic analysis was performed to quantify the amount of impurities, such as loose linkers or adsorbed water.

Scale-up was done by scaling the amounts of all compounds up by a factor 4. For this, 5,1206 g of nickel acetate tetrahydrate was weighed and mixed in 200 mL deminwater, while 1,9666 g of 2,5 g of 2,5-dihydroxyterephthalic acid was weighed and mixed with 200 mL deminwater. After letting both stir until the nickel acetate was fully dissolved, both mixtures were added in a 1L round bottom flask. This time, it seemed the suspension only partially dissolved after mixing. Due to technical difficulties, the mixture was left to stir for three days at room temperature, before being left to stir at 110°C overnight. The resulting suspension was washed using water, where the solid powder was separated from the suspension by using a centrifuge at 6000 rpm for 20 minutes, decanting the liquid phase for as much as possible. Clean water was added and the powder was dispersed, repeating the centrifuge for another 20 minutes at 6000 rpm. This decanting and centrifuging cycle was repeated once more. The last step involved the same cycle, but with clean ethanol added instead.

The weight of the scaled-up sample was 2,8418 g, which can be used to calculate the yield, once the amount of adsorbed water can be calculated.

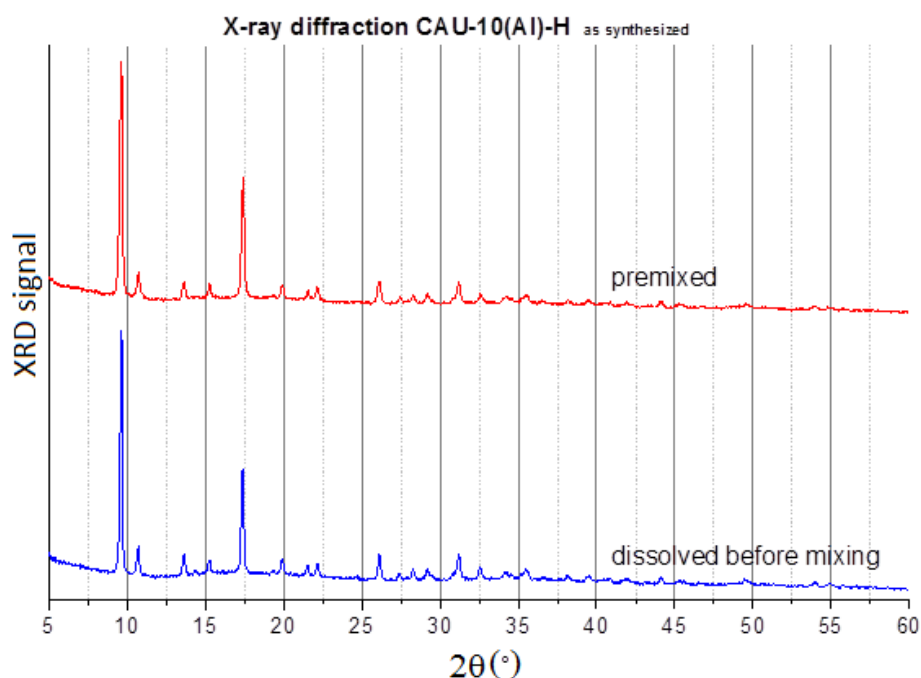
Table S - 3 shows the masses used for all the CPO-27(Ni) samples synthesized, with a yield calculation for every synthesis, based on the amount of moles of bound linker divided by the amount of added linker

4

Characterization

To characterize the MOFs, and X-ray diffraction (XRD) was first performed and compared to the literature to test the crystalline structure. An Infrared (IR) spectroscopy was performed to measure the presence of larger amounts of impurities, by measuring the absorption. This was followed by a thermogravimetric analysis (TGA) to more precisely assess the presence of impurities. A scanning electron microscope (SEM) was used to see the shape of the MOF crystals and to estimate the size.

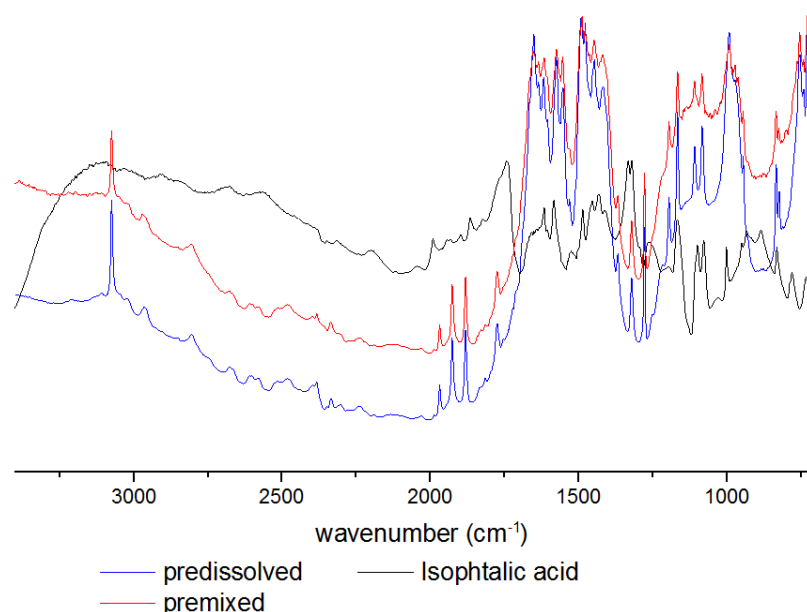
4.1. Characterization of CAU-10(Al)



Graph 2 X-ray diffraction of CAU-10(Al), premixed (above) and dissolved before mixing (below). The similarities in peaks indicate that the two batches have a similar crystal structure.

From the XRD diffractions of the two samples reveal that the crystalline structures are similar to one another. It also indicates that there is no measurable impurity in the mixture, since this resembles the would-be XRD spectrum of CAU-10(Al)-H^[10]. This indicates that the product isn't affected by this difference of synthesizing.

Infrared spectroscopy of CAU-10(Al)-H as synthesized



Graph 3 FTIR absorbance spectroscopy of the premixed (red) and predissolved (blue) samples, as compared to isophthalic acid (black).

Graph 3 is the infrared spectroscopy of the two CAU-10 samples: premixed and predissolved, along with a spectroscopy of isophthalic acid. The sharp peak at 3000 cm⁻¹, as seen on both sample spectra, represents a vibration of an OH-group that is not interacting with other OH-groups (hydrogen bonds), since hydrogen bonding would broaden this peak. This could be the OH-group as seen in the molecular structure: Al(C₈O₄H₄)OH, since that OH group is not surrounded by any hydrogen bonding functional groups, and cannot form hydrogen bonds with solvent material due to steric hindrance. Isophthalic acid's broad peak with its peak around 3000 cm⁻¹ represents a hydrogen bonding –OH group, most likely the –OH group in the carboxylic (-COOH) groups, since these two groups are the only groups in the molecule. These two functional groups form hydrogen bonds with other isophthalic acid molecules.

A small indentation can be seen around the sharp peak at 3000 cm⁻¹ of both MOFs, slightly larger for the sample synthesized by dissolving the salt and linker before mixing, which indicates there's some loose linker present, but nothing conclusive regarding this can be made with just this data.

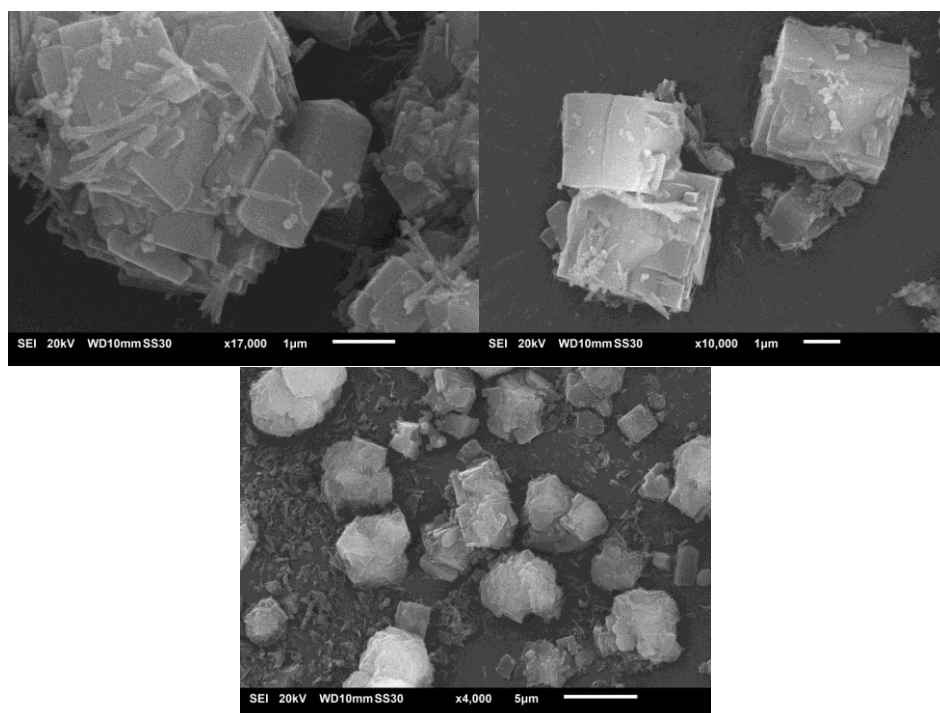
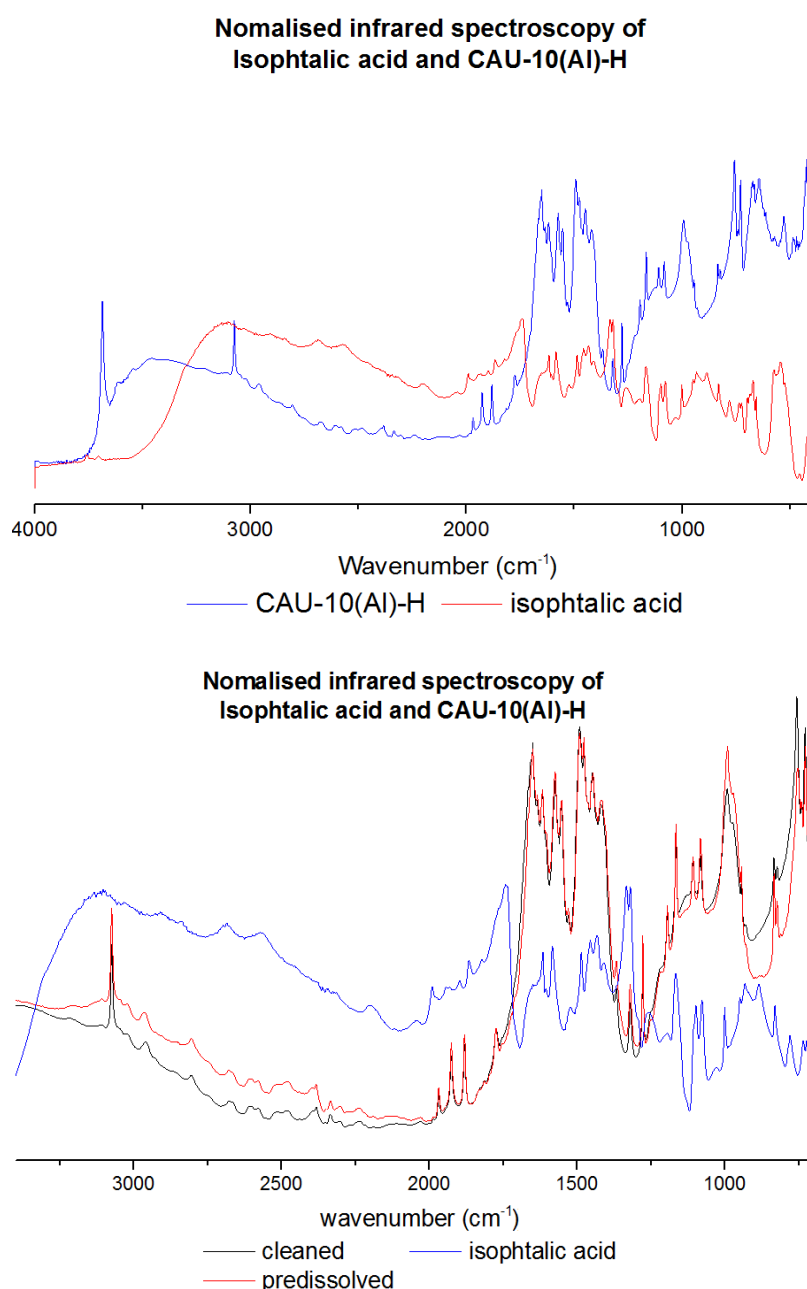


Figure 7 Above: SEM pictures of the predissolved sample; below: SEM picture of the premixed sample. The tiny crystals scattered across the picture indicates the presence of an impurity.

In **Figure 7**, the SEM pictures of both samples can be seen, as these were synthesized, i.e. without washing. It's likely that the cubic crystals are CAU-10(Al)-H, while the much smaller crystals (most visible on the left side of **Figure 7**, below) could be unreacted loose linker. This indicates a need that further washing is needed.

The highly similar spectra of the two samples indicates that the two differences of synthesizing have a negligible effect to the end product, so it was chosen to combine the two samples, to increase the total mass of the combined sample.

Washing was done by dispersing the powder in a mixture of 50% (volume/volume) of DMF in water, and centrifuging at 6000 rpm for 20 minutes, decanting the liquid phase for as much as possible without losing too much of the pellet. This was repeated once more, followed by using ethanol and centrifuging once more at the same settings. The suspension paste was then placed in a drying oven (air at 80°C) overnight, before being placed in glass sample holders.



Graph 4 Top: : the spectra of cleaned CAU-10(Al) and isophthalic acid ranging from 400 to 4000 cm⁻¹ ; Bottom: IR spectroscopy of uncleaned CAU-10 (red), cleaned CAU-10 (black) and isophthalic acid (blue), ranging from 4000 to 1400 cm⁻¹

From the IR spectroscopy as seen in **Graph 4**, it seems that the indentation around 3000 cm^{-1} is not visible anymore, while the rest of the peaks have, although slightly changed in ratio, been left unaffected. This seems to indicate that any loose linkers have been washed out. Another spectrum has been made to give a better overview. The broad peak found in the CAU-10 sample represents the hydrogen bound vibrations of adsorbed water in the MOF and are not indicate a presence in loose linker.

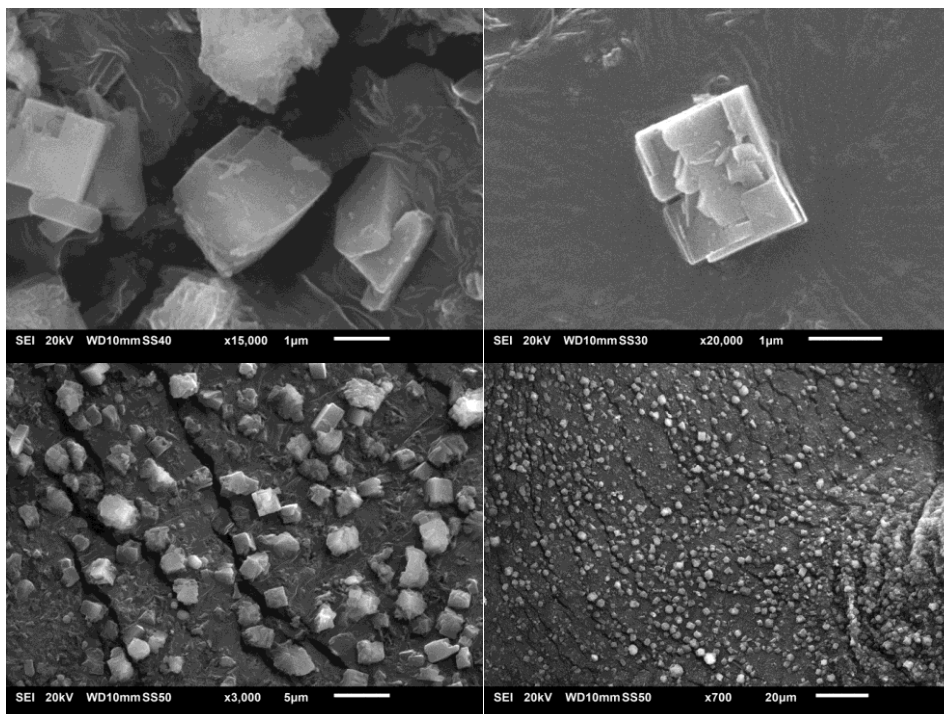
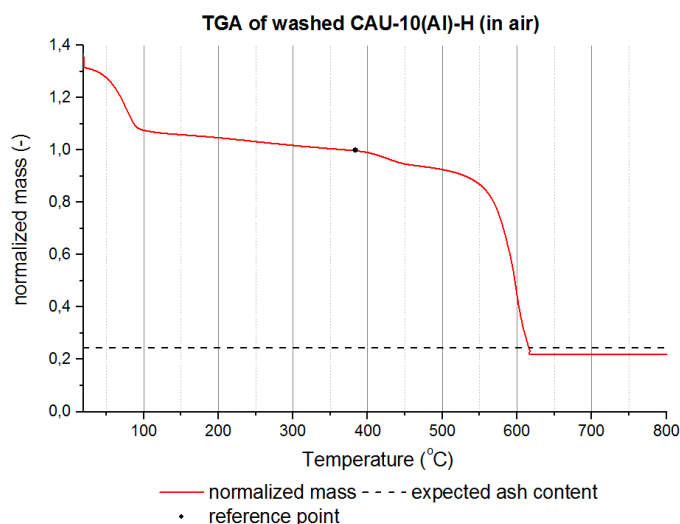


Figure 8 Top: SEM pictures of singular crystals of the cleaned CAU-10(AI) sample, after cleaning with DMF/ethanol; Bottom: Zoomed out SEM pictures of the cleaned CAU-10(AI) sample, after cleaning with DMF/ethanol

Figure 8 Shows that the small crystals are not found anymore. This could imply that the loose linker has been washed out, and only CAU-10(AI) remains.



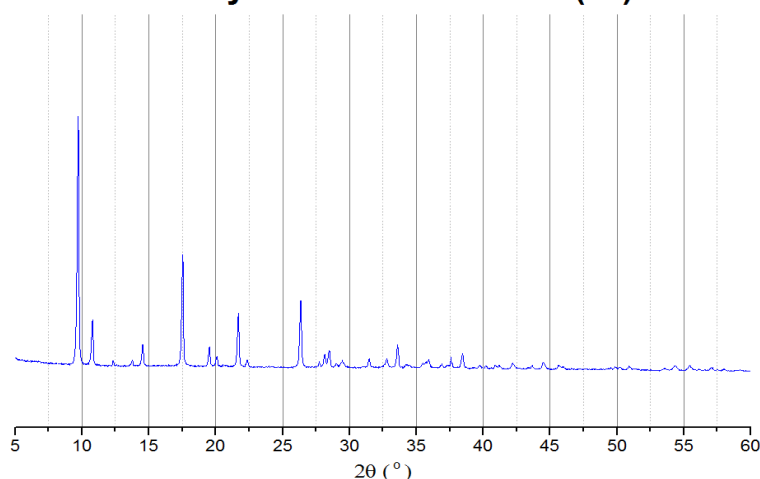
Graph 5 TGA of cleaned CAU-10(AI) in air, with a heating rate of $10^{\circ}\text{C}\cdot\text{min}^{-1}$. The mass has been normalised to measured mass just before the small mass decrease around 400°C (indicated by a black dot). The dashed line represents the expected remaining ash content, based on the mass at the reference point

The TGA as seen in **Graph 5** is a plot of the Thermogravimetric analysis of the CAU-10, under air and a heating rate of $10^{\circ}\text{Cmin}^{-1}$. From this, the water desorption can clearly be seen between 30 and 100°C . The small drop of mass at 400°C indicates the initial decomposition of the MOF's structure, of which a point just before this decrease was used as a reference point for normalisation. The bigger drop at 550°C indicates the full oxidization of the framework into gasses and alumina. The calculated alumina corresponded with the measured remaining ash, within the error of the weighing scale.

From this, it can be concluded that no loose linker is present in the sample after cleaning, as this would be visible as a big drop in mass, a bit before the drop due to oxidation of the MOF.

4.2. Characterization MIL-160(Al)

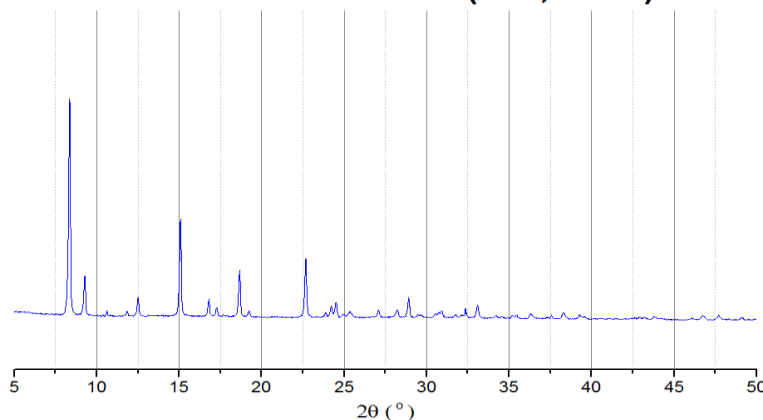
X-ray diffraction MIL-160(Al)



Graph 6 X-ray diffraction of MIL-160(Al), as synthesized

The XRD diffraction pattern as seen in **Graph 6** shows a diffraction pattern of MIL-160(Al), which is very similar to the documented spectrum^[9], though all peaks seem off by a certain factor. This could be because the photon source of the used X-ray diffractometer (Brucker Advance D8) was Cobalt $K\alpha$ radiation ($\lambda = 1,79 \text{ \AA}$), while the documented X-ray source was Copper $K\alpha$ radiation ($\lambda = 1,54 \text{ \AA}$). After applying a correction factor of $1,54/1,79$, the resulting spectrum is in accordance with the documented spectrum, as seen in **Graph 7**.

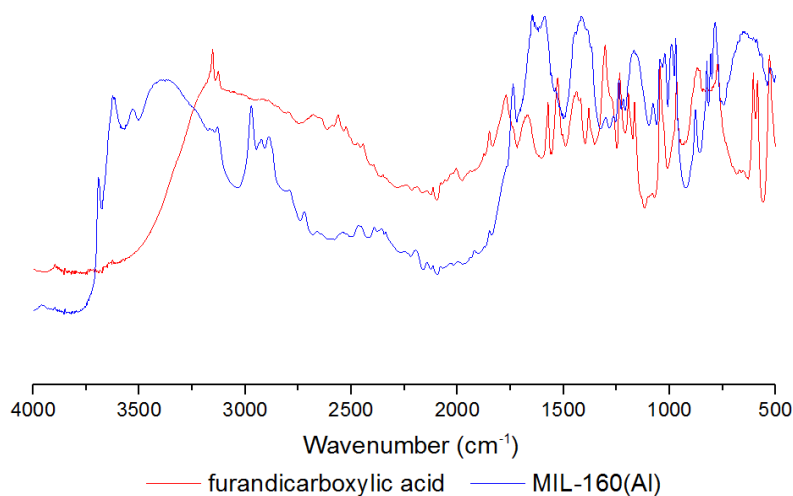
X-ray diffraction MIL-160(Al) corrected for Cu- $K\alpha$ ($\lambda=1,54\text{nm}$)



Graph 7 X-ray diffraction of MIL-160(Al), corrected for the X-ray source ($x_1 = x_0 \cdot 1,54 / 1,79$)

From the XRD spectrum, it can be seen that no crystalline impurities are in the sample, though amorphous impurities will not be detected by means of XRD.

Normalised infrared spectroscopy of 2,4-furandicarboxylic acid and MIL-160(Al)



Graph 8 infrared spectroscopy of MIL-160(Al) and furandicarboxylic acid, over a range between 500 cm^{-1} and 4000 cm^{-1}

Graph 8 is an infrared spectroscopy of the MIL-160(Al) sample, with furanicarboxylic acid, it's organic linker. From this infrared spectroscopy. The similarities in the peaks at the wavenumbers below 2000 cm^{-1} indicates that the linker has remained intact. The broad peak around 3000 cm^{-1} in the spectrum of furandicarboxylic acid represents vibrations in the $-\text{COOH}$ groups, hydrogen bound to the other organic molecules. The broad peak in the spectrum of MIL-160(Al) around 3500 cm^{-1} represents the vibrations coming from adsorbed water molecules, which forms hydrogen bounds with the other water molecules and the MOF. The two sharp peaks around 3200 cm^{-1} (visible in both the spectrum of the MOF and that of the linker) could represent the vibration in the C-H functional group in the furan ring. The two sharp peaks around 3700 cm^{-1} represent the vibration of the OH group, as seen in the molecular formula: $\text{Al}(\text{C}_7\text{O}_5\text{H}_2)\text{OH}$.

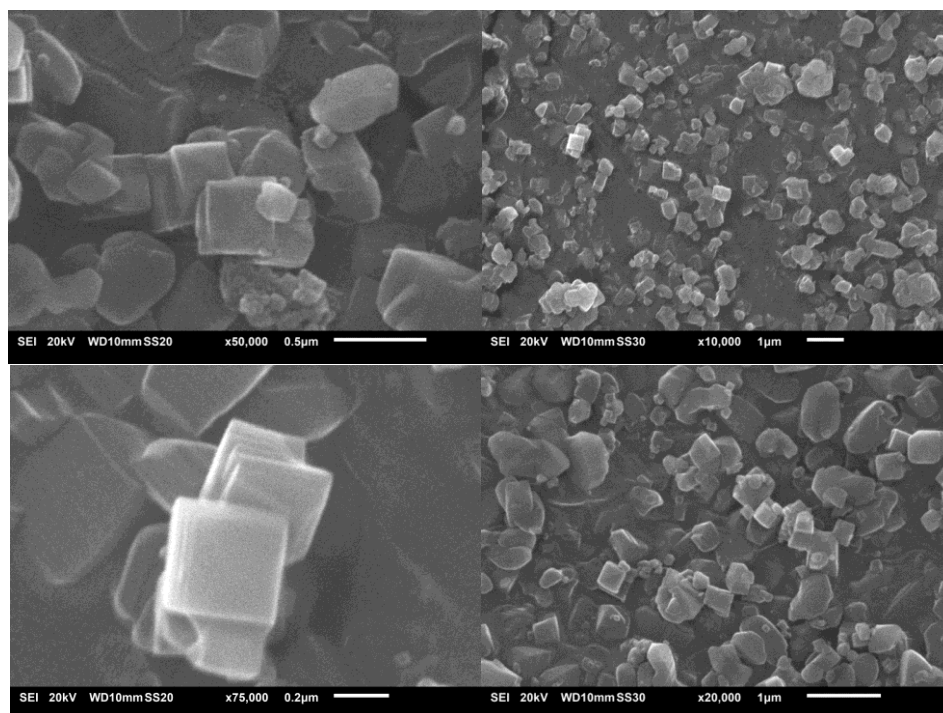
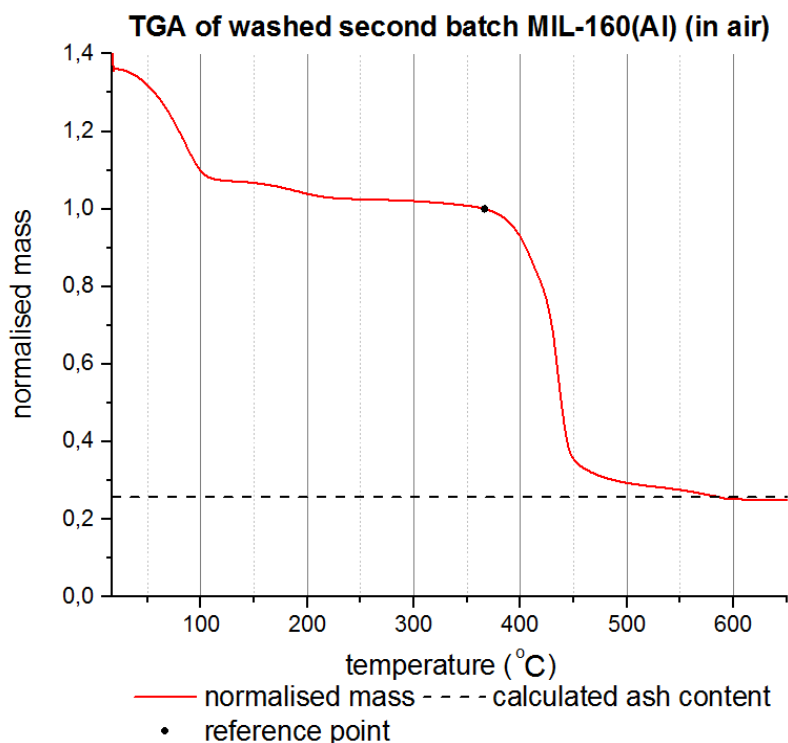


Figure 9 Scanning electron microscope pictures of the MIL-160(Al) crystals; more zoomed in (left) and more zoomed out (right)

Figure 9 shows four Scanning Electron Microscope pictures made of the MIL-160(Al) sample. From these pictures, it can be seen that the size of the cubic crystals are significantly smaller than CAU-10(Al), with their sizes being around 0,2 μ m. Apart from the small crystals, nothing was found, which might mean that this MOF could be clean of any loose linker, though nothing can be concluded with just this data.



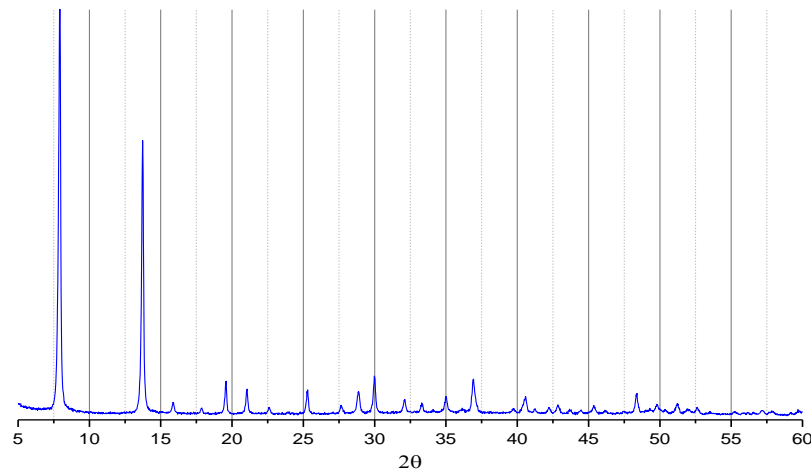
Graph 9 Thermographic analysis of MIL-160(Al), normalised to the reference point; the dashed line represents the calculated ash content, based on alumina ash and the mass at the reference point

From the TGA of MIL-160(Al), as seen in **Graph 9**, shows a large decrease in mass until 100°C, which is likely desorption of water. The small decrease until 200°C is likely DMF used in cleaning the sample. The large drop in mass around 400°C comes from burning the linker, leaving alumina as its ash. Therefore, a measurement point just before the large mass drop is used as its reference point.

The amount of ash that is expected to be left per gram of MOF would be equal to the ratio between the molar mass between alumina and the MOF itself: $50,982 / 198,066 = 0,257$ grams per gram of sample. As is visible, no excess amount of thermally stable products are left and no loose linker is left, as this would result in a larger difference between the calculated amount and the measured amount at high temperatures or another drop in mass just before the large drop measured, respectively.

4.3. Characterization of CPO-27(Ni)

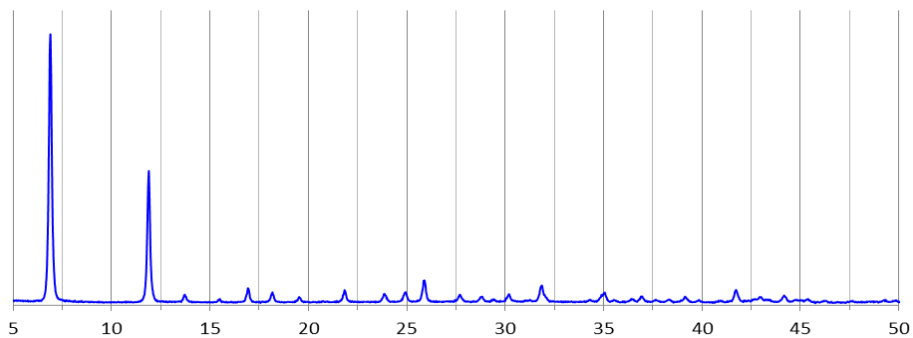
X-ray diffraction CPO-27(Ni)



Graph 10 X-ray diffraction of CPO-27(Ni)

The XRD diffraction pattern as seen in **Graph 10** shows a diffraction pattern which is very similar to the documented spectrum^[11], but all peaks seem off by a certain factor. This is, because the photon source of the used X-ray diffractometer (Brucker Advance D8) was Cobalt $K\alpha$ radiation ($\lambda = 1,79 \text{ \AA}$), while the documented X-ray source was Copper $K\alpha$ radiation ($\alpha = 1,54 \text{ \AA}$). After applying a correction factor of $1,54/1,79$, the resulting spectrum is in accordance with the documented spectrum, as seen in **Graph 11**.

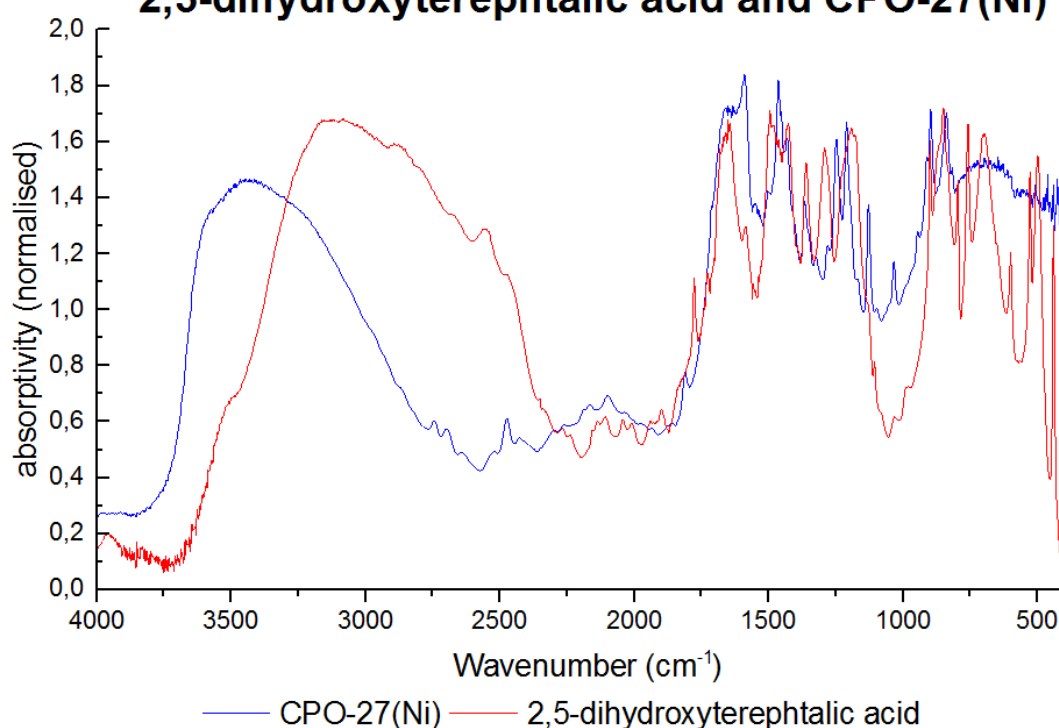
XRD CPO-27(Ni) (corrected for Cu $K\alpha$)



Graph 11 XRD spectrum of CPO-27(Ni), corrected for the radiation source ($x_1 = x_0 \cdot 1,54 / 1,79$)

From both XRD spectra, it can be seen that no crystalline impurities can be found, but any amorphous impurities will not be measurable from XRD.

Normalised infrared spectroscopy of 2,5-dihydroxyterephthalic acid and CPO-27(Ni)



Graph 12 Infrared spectra of CPO-27(Ni), as compared to that of its used organic linker: 2,5-dihydroxyterephthalic acid; the spectra have been normalised based on the average values along the measured spectrum

Graph 12 is the infrared spectrum of CPO-27(Ni) and that of 2,5-dihydroxyterephthalic acid, the organic linker. As is visible, the spectra of the linker and the MOF are similar for wavenumbers $< 2000 \text{ cm}^{-1}$, which seems to indicate that the molecular structure of the linker remained intact during the reaction, meaning the bound linker is probably 2,5-dihydroxyterephthalate. The absence of the broad peak around 3000 cm^{-1} in the spectrum of CPO-27 indicates that no more loose linker is to be found in the MOF, as his broad peak represents the vibrations between hydrogen bound $-\text{COOH}$ groups. The broad peak around 3500 cm^{-1} in the spectrum of CPO-27(Ni) indicates hydrogen bound $-\text{OH}$ groups, which can be explained by the presence of ads- and chemisorbed water. Because the MOF itself does not have any $-\text{OH}$ groups (unlike CAU-10(Al)), this would imply an absence of any sharp peaks around that area, which were visible with the spectrum of CAU-10(Al). This is in accordance with the measured spectrum.

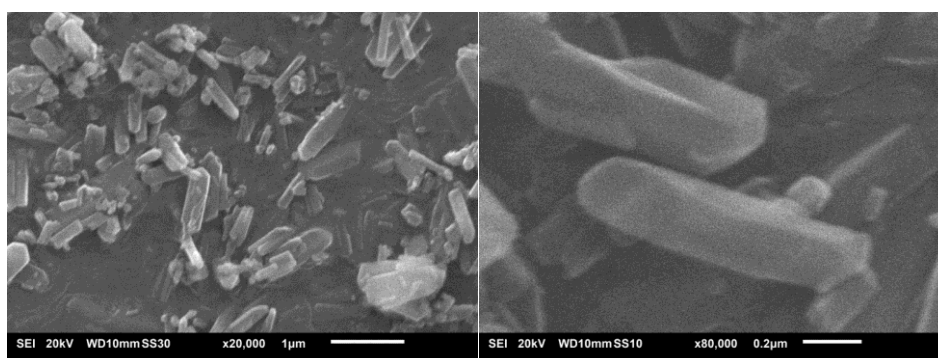
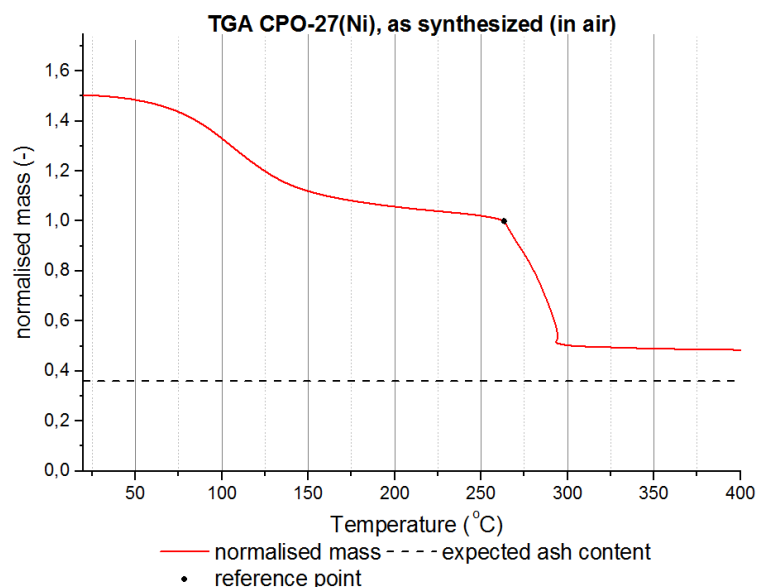


Figure 10 SEM pictures of CPO-27(Ni), a more zoomed out picture (left) and zoomed in to a singular crystal (right)

As seen in **Figure 10**, the crystals of CPO-27(Ni) are significantly smaller as compared to that of the MOF CAU-10(Al), with its crystal size being approximately $0,2 \mu\text{m}$ in width and $1 \mu\text{m}$ in length. Because of this much smaller size, nothing significant can be said about any possible presence of loose linker.



Graph 13 Thermographic analysis of as-synthesized CPO-27(Ni) with a heating rate of $10^{\circ}\text{C}\cdot\text{min}^{-1}$. The mass has been normalised to the measured mass just before the steep decrease around 250°C (indicated by a black dot). The dashed line represents the expected remaining ash content, based on NiOOH ash and the mass at the reference point

As seen in [Graph 13](#), CPO-27(Ni) seems to adsorb a lot of water until a bit more than 250°C , where the MOF seems to burn until only ash remains.

From this performed TGA, it seemed that the resulting powder was black. This indicates that the ash formed is not nickel oxide (NiO), as this is a green substance, but likely black nickel oxide hydroxide (NiOOH). The molar mass of this substance is $97,701\text{ g/mol}$, while that of CPO-27(Ni) is $254,807\text{ g/mol}$. This means that for one gram of the MOF, $97,701/254,807 = 0,35988$ grams of ash will be left per gram of dry sample. This is indicated by the black horizontal line in [Graph 13](#).

From this, it can be seen that there is still some uncoordinated nickel, which is likely to be in the form of unreacted nickel acetate. This means that additional cleaning is required using water.

5

Activation of the MOFs and adsorption

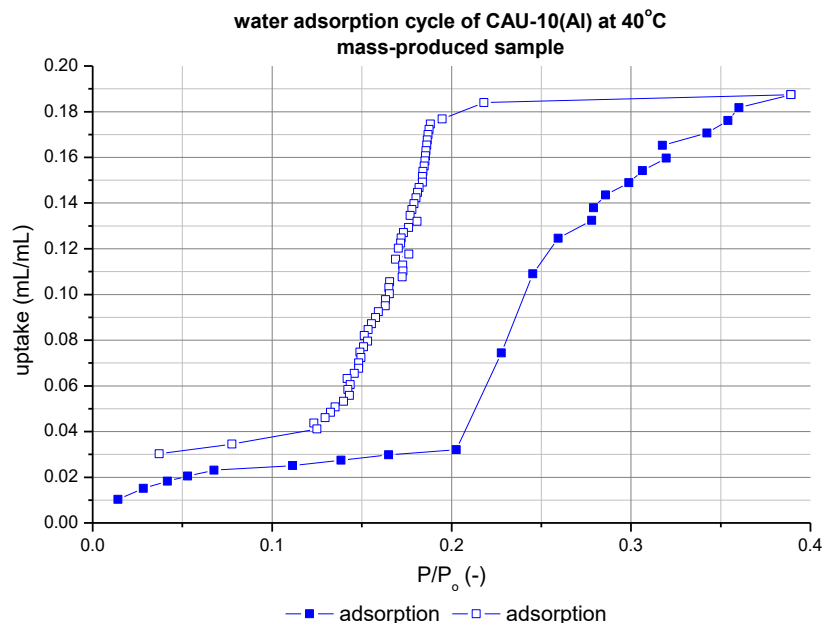
To measure the adsorption, both the water and nitrogen adsorption was measured. For the adsorption of nitrogen, a MicroMeretics Tristar II was used, under liquid nitrogen to keep the temperature constant at 77 K. around 100 mg was weighed in the sample holder and placed in the setup.

To measure the water adsorption, a Quantachrome Vstar was mainly used, where around 100 mg was weighed into a sample holder and placed in the setup, measuring at 25, 40 and 60°C, along pressures between 0 and 50% of the water vapour pressure at the measured temperature

In some occasions, the MicroMeretics Tristar II was used, but because the MicroMeretics cannot heat the whole setup, but only the sample holder. Therefore, the MicroMeretics was only used for measuring at 40°C, measuring in an interval between 0 and 40% of the water vapour pressure.

5.1. CAU-10(Ni)-H

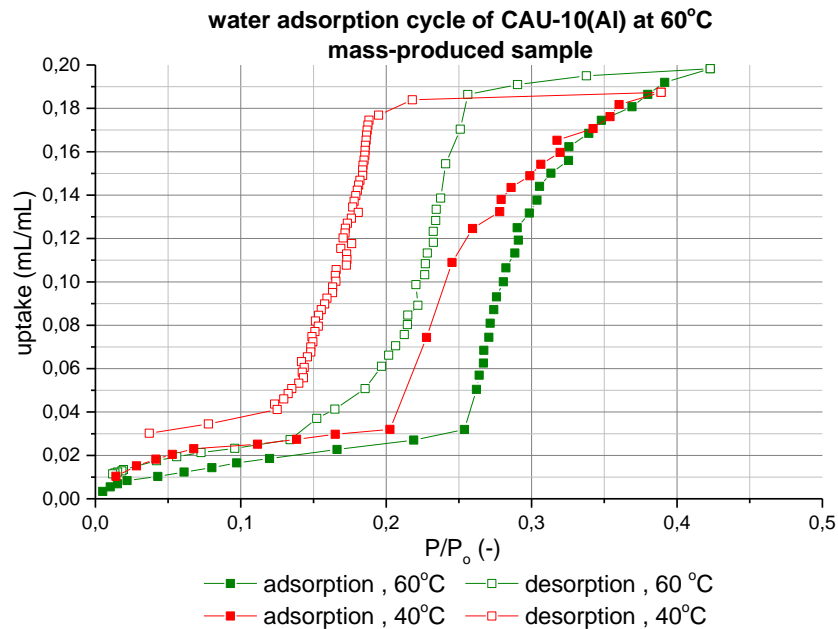
For the water adsorption, a temperature of 40°C was first chosen for CAU-10(Al), since this temperature was modelled to be the better temperature for water adsorption. For pragmatic reasons, the mass-produced sample was chosen, simply for having more mass of said sample to work with.



Graph 14 Water adsorption measured using the Quantachrome sorption analyser., measured over $0 < P/P_0 < 0,4$. The closed symbols indicate adsorption, while the open symbols represent desorption.

Graph 14 shows the water adsorption isotherm of this sample at 40°C, between $P/P_0 = 0$ to 0,4 . Because the “jump” in water adsorption what will be discussed, measuring beyond $P/P_0 = 0,4$ would not be as relevant.

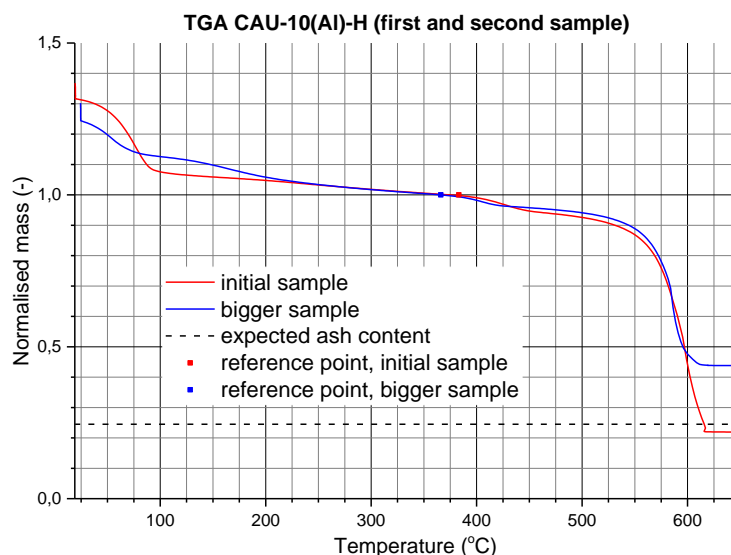
From the plot, it can be seen that the adsorption of water deviates a from the modelled value, while the desorption seems closer to what is measured. The isotherm does seem to show a strong hysteresis between adsorption and desorption. This could be due to mass transport limitations, but the lack of significant data points in the water adsorption seems to come from a bug in the software from the sorption analyser, resulting in the measurement points cutting short, before an equilibrium has been reached. This could also explain the deviation.



Graph 15 Water adsorption measured using the Quantachrome sorption analyser, a comparison of the isotherms at the temperatures 40°C (red) and 60°C (green), both measured over $0 < P/P_0 < 0.4$. The closed symbols indicate adsorption, while the open symbols represent desorption.

Graph 15 shows the same sample, but measured at a temperature of 60°C. As compared It seems that the measured adsorption is lower than is expected. This could be because, unlike the initial sample, this sample does indeed contain impurities, despite the similar synthesis. To measure this, a TGA was performed on the sample, and a nitrogen adsorption isotherm (kept at 77K using boiling nitrogen) was attempted.

The nitrogen adsorption yielded no reliable results, since the kinetics of the adsorption was too slow for any significant measurements to be made before the liquid nitrogen ran out. This indicates strong clogging of the pores, which means that there should be a presence of impurities.



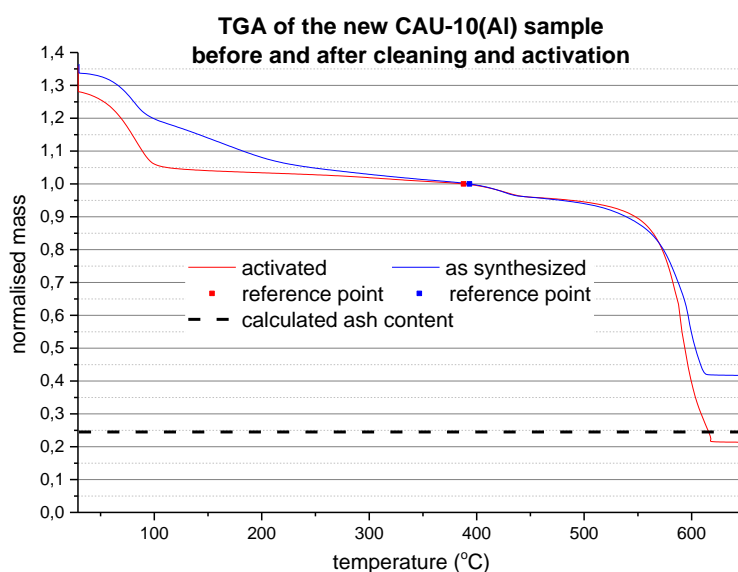
Graph 16 Thermographic analysis of both the initially synthesized sample and the larger sample. The mass has been normalised to measured mass just before the small mass decrease around 400°C (indicated by a black dot). The dashed line represents the expected remaining ash content, based on the mass at the reference point.

From the TGA performed, it can be seen that a relatively large amount of remaining ash is found. It was initially thought to be unreacted aluminium sulphate, but after washing with both water and DMF, this excess amount of ash remained, so it can hereby be concluded that it must be something which is non-soluble. Hypothesized is that it could be alumina, but this is not clear. Because of this, no more measurements were performed using this sample.

To increase the amount of CAU-10(Al), it was chosen to redo the initial synthesis thrice, rather than using a larger volume. These samples were tested separately using infrared spectroscopy to determine any differences in the product, as can be seen in the appendix (**Graph S - 1**).

Although the spectra seem very similar to the initially measured spectrum of CAU-10(Al), a few additional sharp peaks can be seen in all samples: most notably around 3700 cm^{-1} and 2900 cm^{-1} . Due to the sharpness of the peaks, it has been assumed that these represent N-H vibrations from adsorbed DMF, since no DMF extraction has been performed prior to measuring the spectrum.

From this, it can be seen that all three samples, although the peak height ratios differ, the position of all peaks are the same and all peaks are present in all three samples. From this, it was concluded that all three samples were the same and could therefore be mixed into one sample holder for convenience.

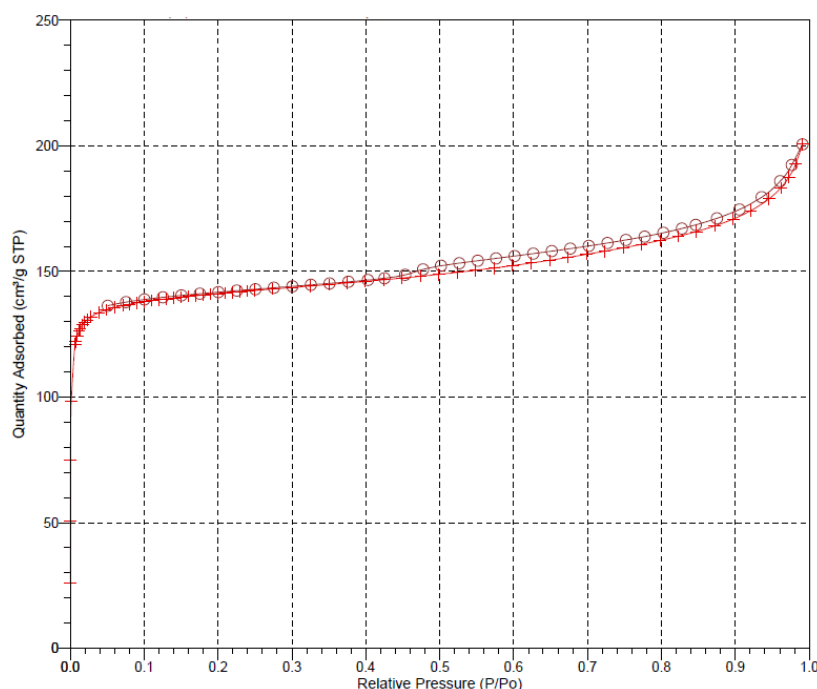


Graph 17 TGA of the new sample before (blue) and after (red) cleaning and activation. Their respective reference points are depicted as squares in the same colour. The mass has been normalised to measured mass just before the small mass decrease around 400°C (indicated by a black dot). The dashed line represents the expected remaining ash content, based on the mass at the reference point.

To remove the DMF, the MOF was washed with water, followed by an activation of the sample at a temperature of 250°C in vacuum, instead of 150°C. This temperature was chosen partially due to the high thermal stability of the MOF.

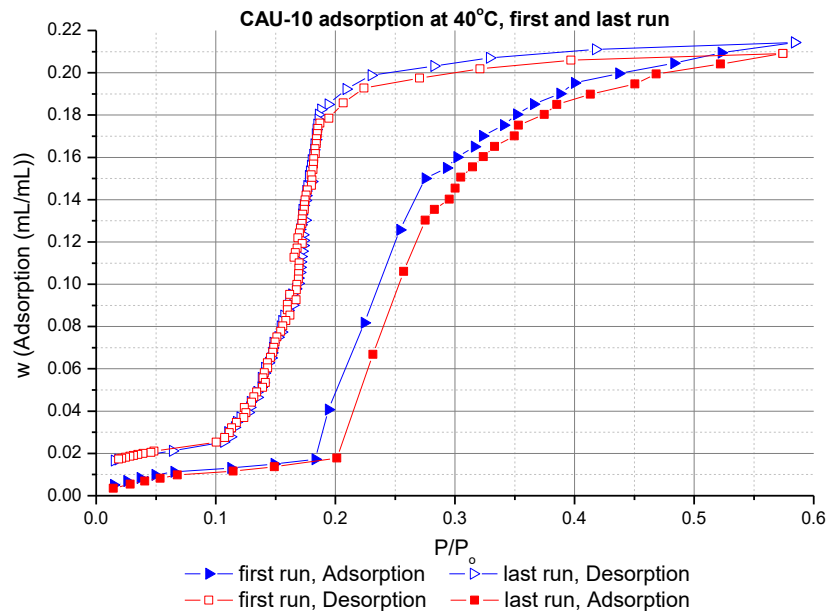
Graph 17 Shows a TGA of the sample, as synthesized and after cleaning. As was expected, the TGA of the sample as synthesized shows a kink in the mass decrease between 100°C and approximately 250°C. This indicates the presence of a substance with a lower volatility than that of water, which is likely to be DMF. The activated CAU-10 does not seem to have this kink, so it can therefore be assumed that all DMF has therefore been removed.

The increased amount of ash remaining in the as synthesized sample indicates that some impurities were present when synthesizing. The absence of any remaining ash in the activated sample indicates that this was probably a water soluble salt (as this would be “flushed” away when cleaning with water), presumably unreacted aluminium sulphate.

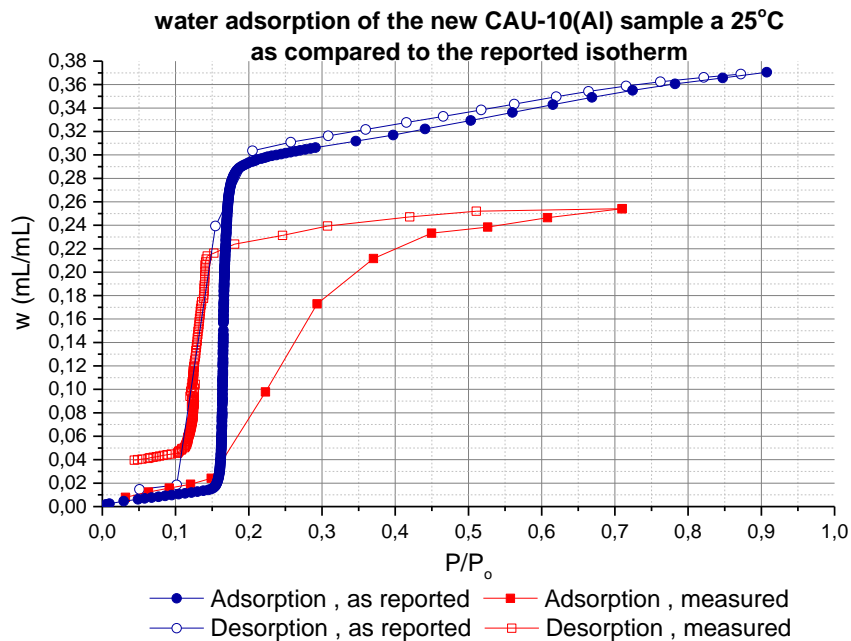


Graph 18 nitrogen adsorption isotherm of the CAU-10(Al) sample after cleaning, performed at 77K. The red plus signs indicate adsorption, while the purple circles indicate the desorption branch.

The nitrogen adsorption isotherm (**Graph 18**) shows that after cleaning, the isotherm was able to complete fully without problems. The adsorption is also what is expected, when comparing the literature values^[12]. This means that this sample is pure enough for water adsorption.



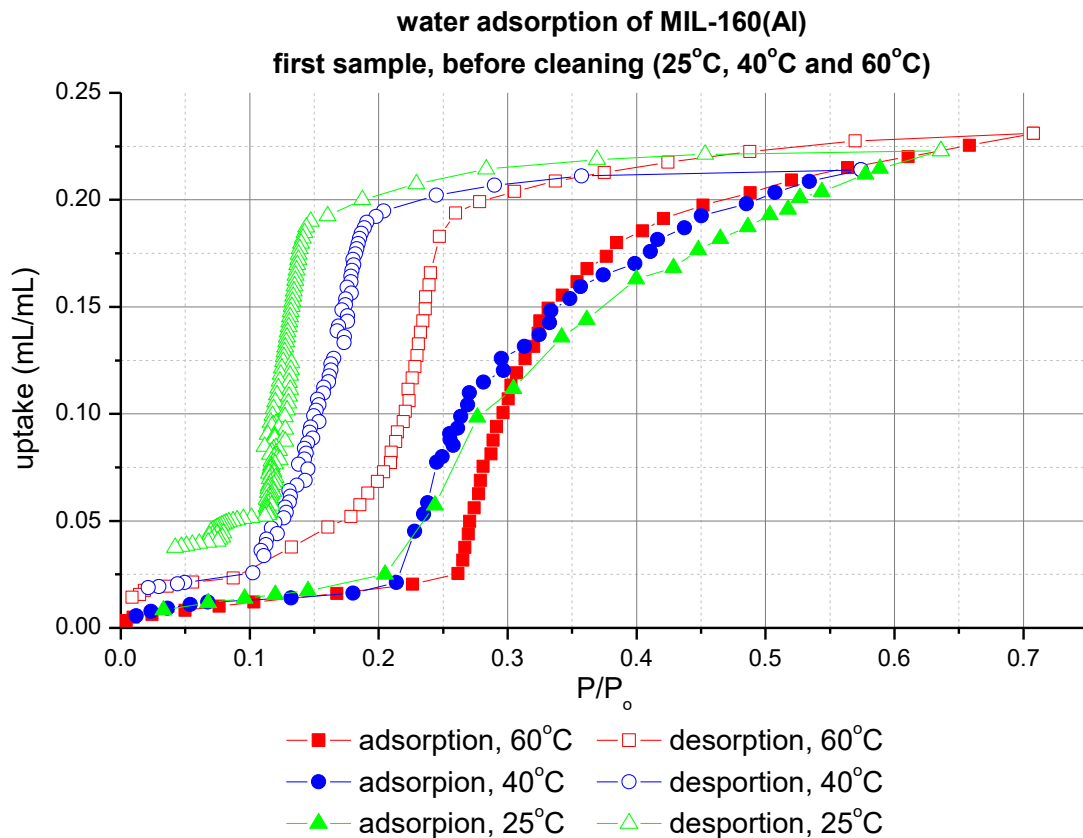
Graph 19 water adsorption isotherm, as performed on the new sample, the first run and the last cycle of the measurement, run over $0 < P/P_0 < 0,6$. The closed symbols indicate adsorption, while the open symbols represent desorption.



Graph 20 water adsorption of the new sample of CAU-10(Al) at 25°C (red), compared to the reported isotherm as performed by de Lange et al. (blue) The closed symbols indicate adsorption, while the open symbols represent desorption.

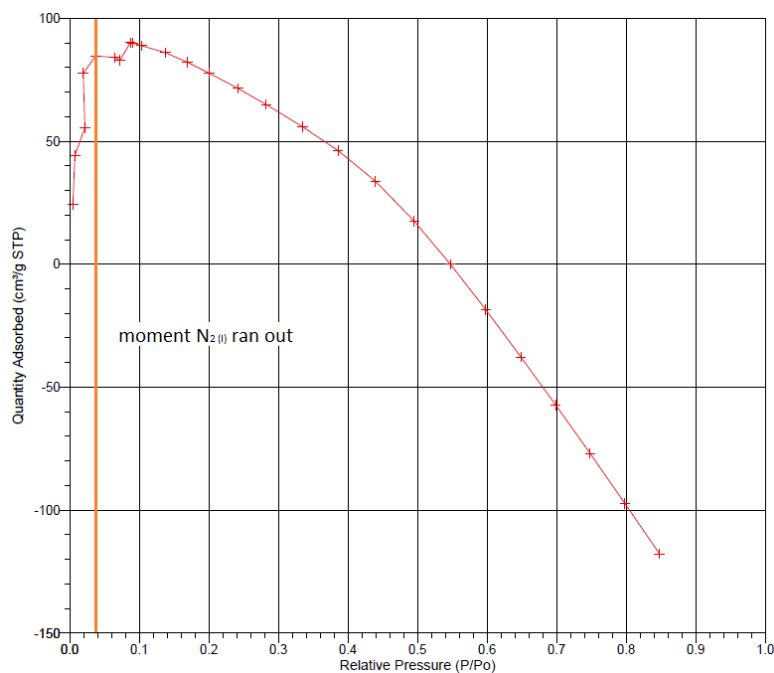
As can be seen in **Graph 20**, the adsorption isotherm of this new sample seems, although slightly higher than previous sample, still be significantly lower than what has been reported. Given that the nitrogen adsorption has yielded adsorption results similar to the reported isotherm, it can thereby be concluded that the isotherm is mostly defined by mass transport limitations, due to the shorter adsorption time given by the Quantachrome.

5.2. MIL-160(Al)



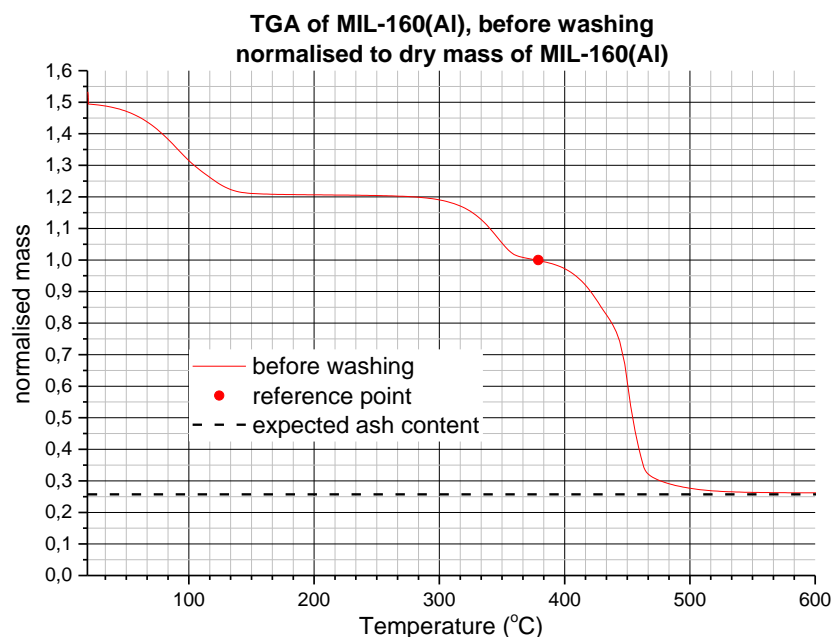
Graph 21 water adsorption isotherms of the first sample at 25°C (green), 40°C (blue) and 60°C (red); the plots can be seen separately in the appendix as **Graph S - 2**, **Graph S - 3** and **Graph S - 4**. The closed symbols indicate adsorption, while the open symbols represent desorption.

As can be seen from **Graph 21**, the water adsorption of MIL-160(Al) seems significantly lower than that of reported values ^[9].



Graph 22 nitrogen adsorption isotherm of the first MIL-160(Al) sample at 77K. The orange line represents the moment in time where the nitrogen tank ran out of liquid nitrogen and hence the temperature could not be kept constant at 77 K.

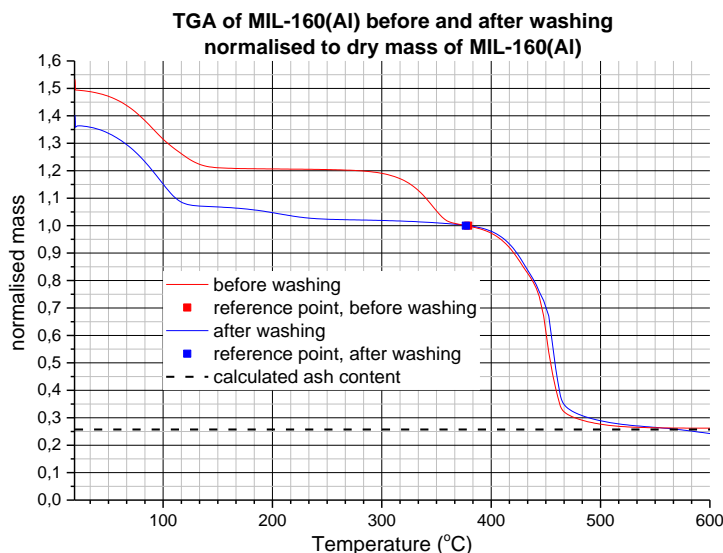
The nitrogen isotherm as seen in **Graph 22** shows very slow adsorption kinetics, to the point of not being able to provide a good enough isotherm, due to the liquid nitrogen running out before anything significant was able to be measured.



Graph 23 TGA of MIL-160(Al), first sample, before washing, normalised to its dry, pure form. The mass has been normalised to measured mass just before the small mass decrease around 400°C (indicated by a black dot). The dashed line represents the expected remaining ash content, based on the mass at the reference point

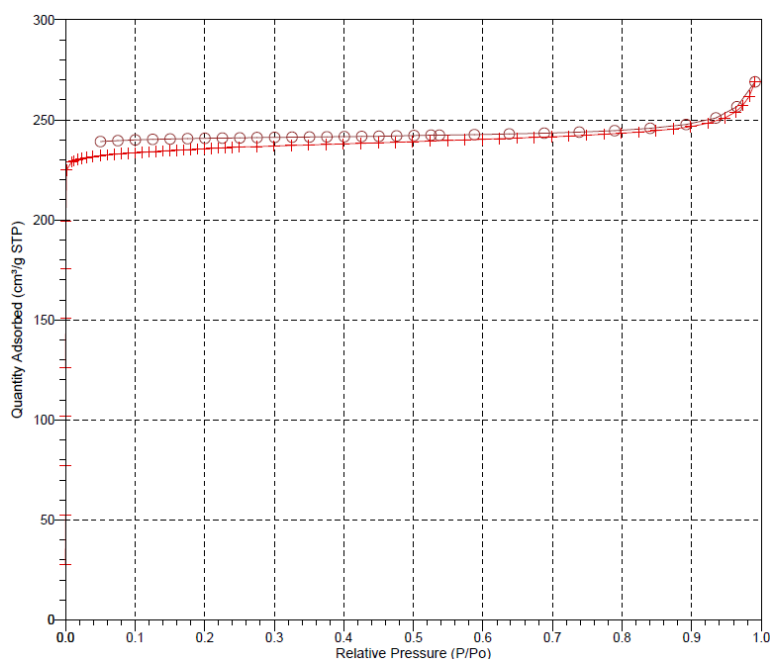
From the TGA seen in **Graph 23**, the sample seems to be contaminated with free furandicarboxylic acid linker. This is visible by the mass drop between 300°C and 360°C. Since the bound linker is expected to be slightly more stable than its free counterpart, this would result in an oxidation temperature of the free linker being which is slightly lower. When normalising to the second drop in mass, it seems that no excess of ash was present in the sample.

Washing of the material was performed by submerging the powder in DMF and keep stirring overnight at 100°C. The powder was then separated from the suspension by centrifuging, followed by submerging the sample in water, stirring in 100°C overnight. The suspension was then centrifuged and decanted. Water was added to the remaining powder and the powder was redispersed before centrifuging and decanting again. This was repeated with ethanol. The remaining powder was dried in an oven at 80°C overnight.



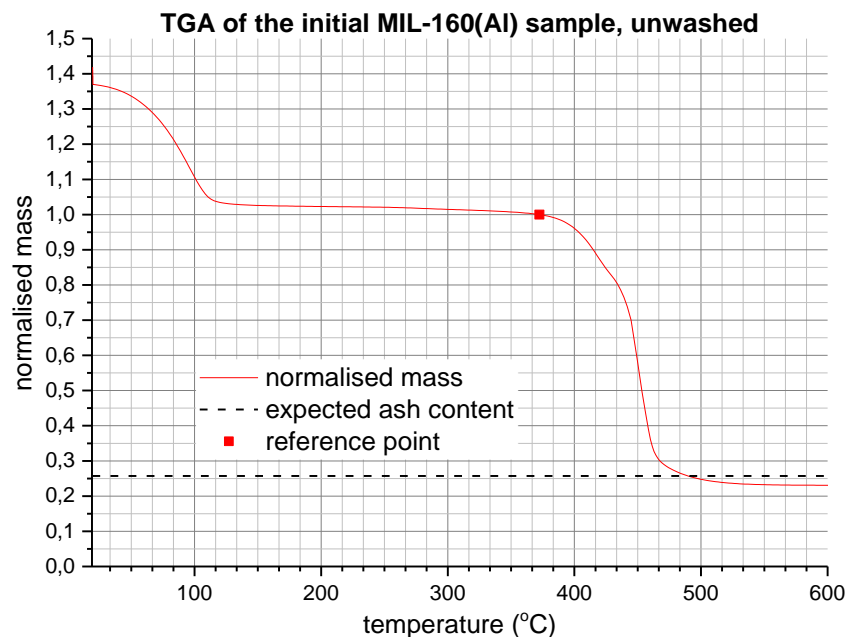
Graph 24 TGA of the sample, before and after washing. The mass has been normalised to measured mass just before the small mass decrease around 400°C (indicated by a black dot). The dashed line represents the expected remaining ash content, based on the mass at the reference point

Graph 24 shows a TGA of the sample, before and after the cleaning procedure. As can be seen, the mass drop representing the free linker is no more visible. The small mass drop around 150°C likely represents the desorption of the remaining DMF, used for cleaning the sample. This DMF should disappear with the next activation overnight in 150°C in vacuum overnight, before the nitrogen adsorption.



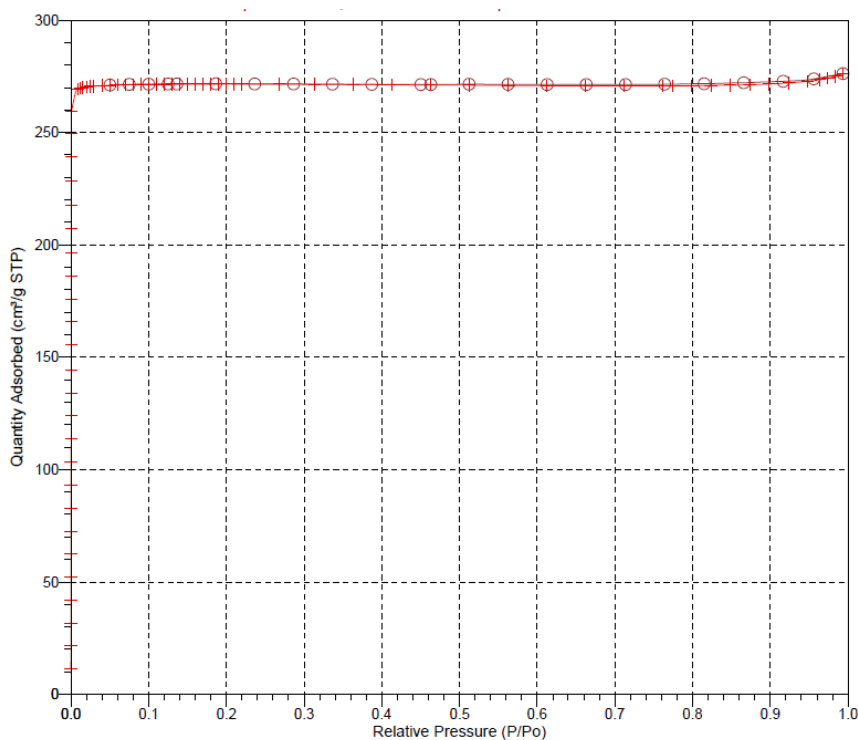
Graph 25 Nitrogen adsorption isotherm of the cleaned sample, at 77K. The red plus signs indicate adsorption, while the purple circles indicate the desorption branch.

The nitrogen adsorption of the sample after cleaning shows an isotherm that more closely resembles that of the literature values^[9], with the BET surface area being around 1000 cm²/g, while the micropore volume being around 0.35cm³/g. This would mean that the sample is clean now, but the cleaning decreased the amount of remaining sample down to approximately 50 mg, which is insufficient to perform a water adsorption spectrum.



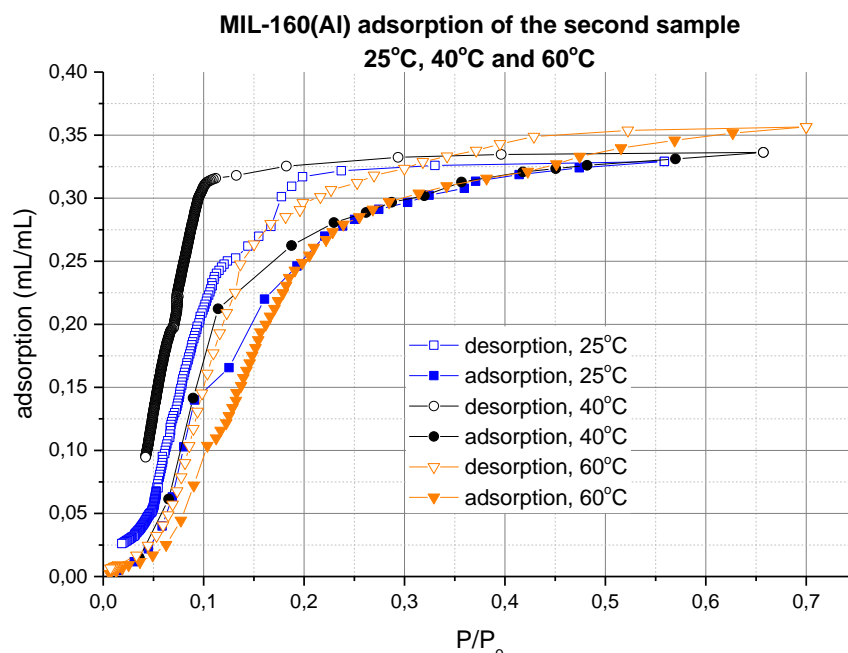
Graph 26 TGA of the third sample, not cleaned. The mass has been normalised to measured mass just before the small mass decrease around 400°C (indicated by a black dot). The dashed line represents the expected remaining ash content, based on the mass at the reference point

From the TGA as seen in **Graph 26**, this new sample is shown to be free of excess ash and free unbound linker. For this reason, no further cleaning was required.

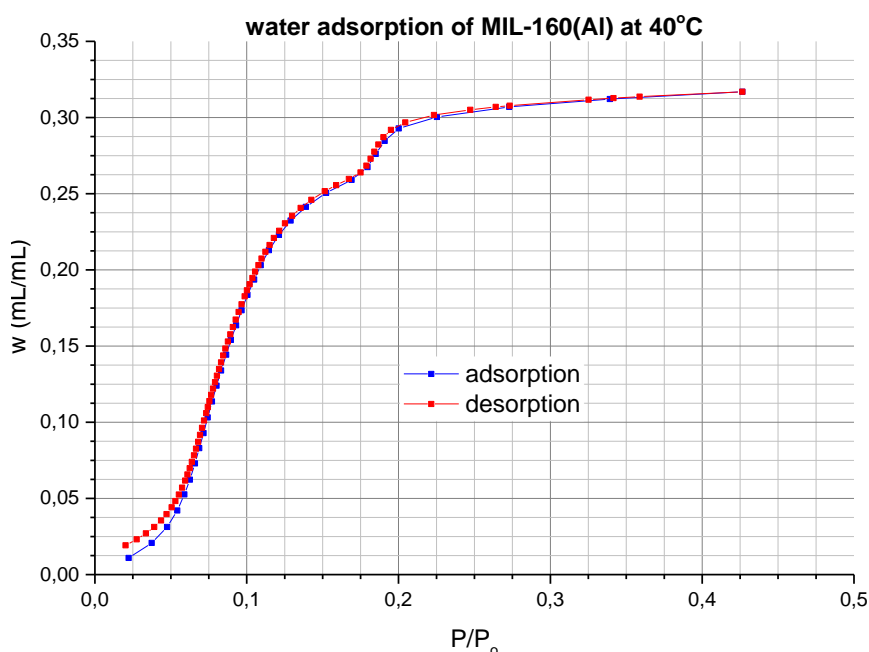


Graph 27 Nitrogen adsorption isotherm of the third sample, performed at 77K. The red plus signs indicate adsorption, while the purple circles indicate the desorption branch.

The nitrogen adsorption as seen in **Graph 27** seems that the third sample has the isotherm that's comparable to that of the reported isotherm, with the BET surface being around 1200 m²/g, and the volume of the micropores being around 0,42 cm³/g



Graph 28 Water adsorption isotherms of MIL-160(Al) in 25°C (blue), 40°C (black) and 60°C (orange) (as performed by the Quantachrome Vstar sorption analyser). The plots can be seen separately in the appendix as [Graph S - 5](#), [Graph S - 6](#) and [Graph S - 7](#). The closed symbols indicate adsorption, while the open symbols represent desorption.

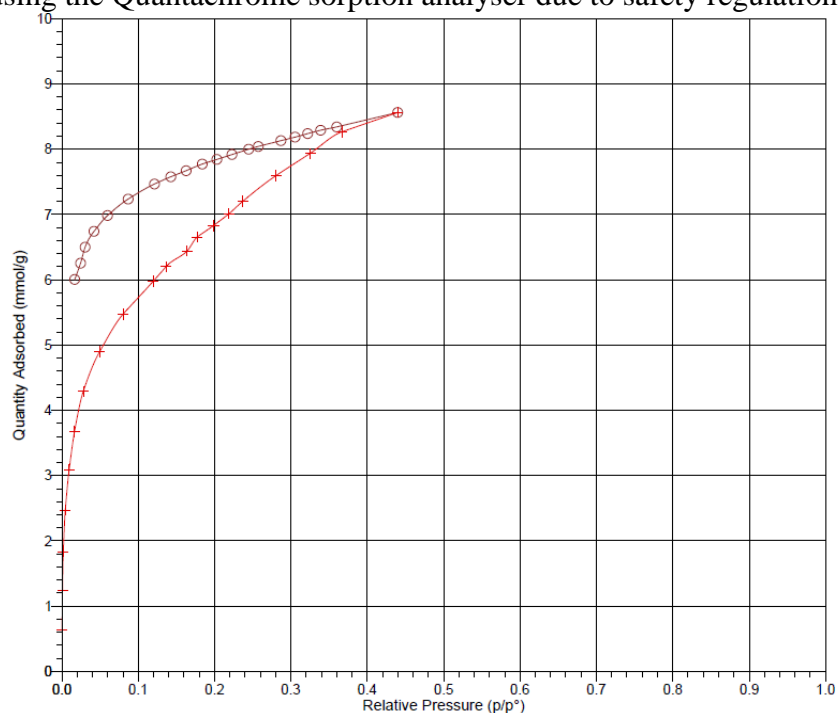


Graph 29 Water adsorption isotherm of MIL-160(Al) in 40°C (as performed by the Micromeritics sorption analyser) The red line indicates desorption, while the blue line represents adsorption.

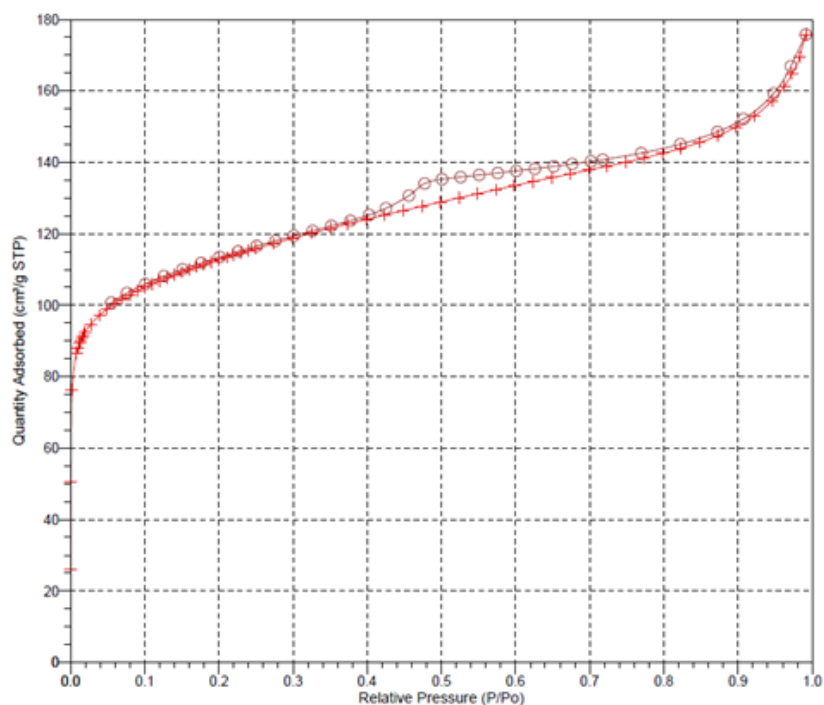
From [Graph 28](#) and [Graph 29](#), it seems that the sample has an adsorption that is similar to what has been recorded in the literature^[9]. The adsorption as performed by the Quantachrome sorption analyser seems on a similar level as compared to isotherm of the Micromeritics sorption analyser, but the Quantachrome yields a significantly larger hysteresis. This is probably because the Quantachrome sorption analyser seems to utilise a lower residence time for the water vapour, which means the adsorption has not yet reached equilibrium. The downside of the micromeritics setup is that only the sample is heated, as opposed to the Quantachrome, which heats the whole system. This means the Quantachrome can measure the isotherm over the whole pressure range until $P/P_0 = 1$, while the Micromeritics can only measure in the range of below $P/P_0 = 0,4$ at a temperature of 40°C to avoid condensation on the setup. It was therefore chosen to take the Quantachrome isotherm as a reference for the energy density measurement.

5.3. CPO-27(Ni)

Because of a lack of any MSDS sheet compatible with CPO-27(Ni), no water adsorption measurement has been performed using the Quantachrome sorption analyser due to safety regulations.



Graph 30 water adsorption of the first sample of CPO-27(Ni), as performed using the Micromeritics sorption analyser at 40°C. The red plus signs indicate adsorption, while the purple circles indicate the desorption branch.

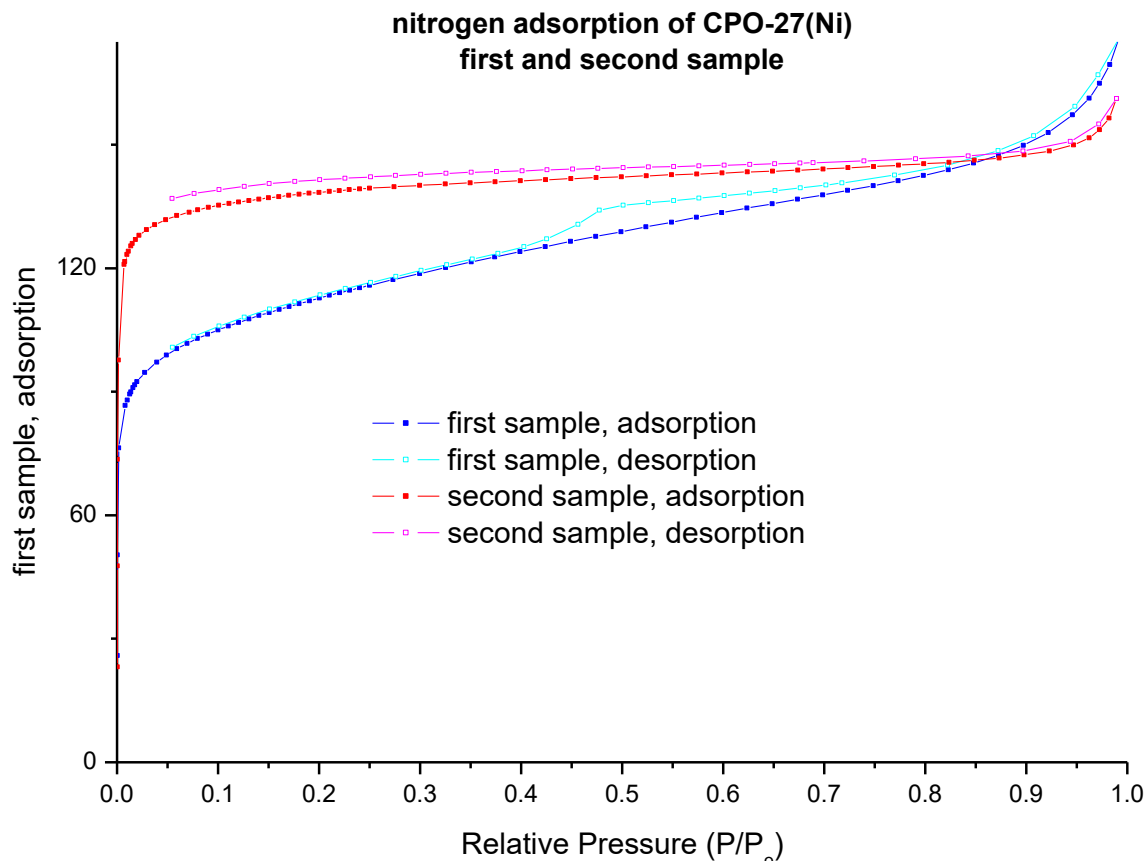


Graph 31 nitrogen adsorption isotherm of CPO-27(Ni), first sample. The red plus signs indicate adsorption, while the purple circles indicate the desorption branch.

As can be seen from **Graph 30**, the water adsorption is significantly lower than that of the expected value^[11]. **Graph 31** shows a nitrogen adsorption isotherm of the same sample. This isotherm seems to indicate that the structure has been damaged, forming nickel oxide nanoparticles within the MOF structure. Since this only happens when

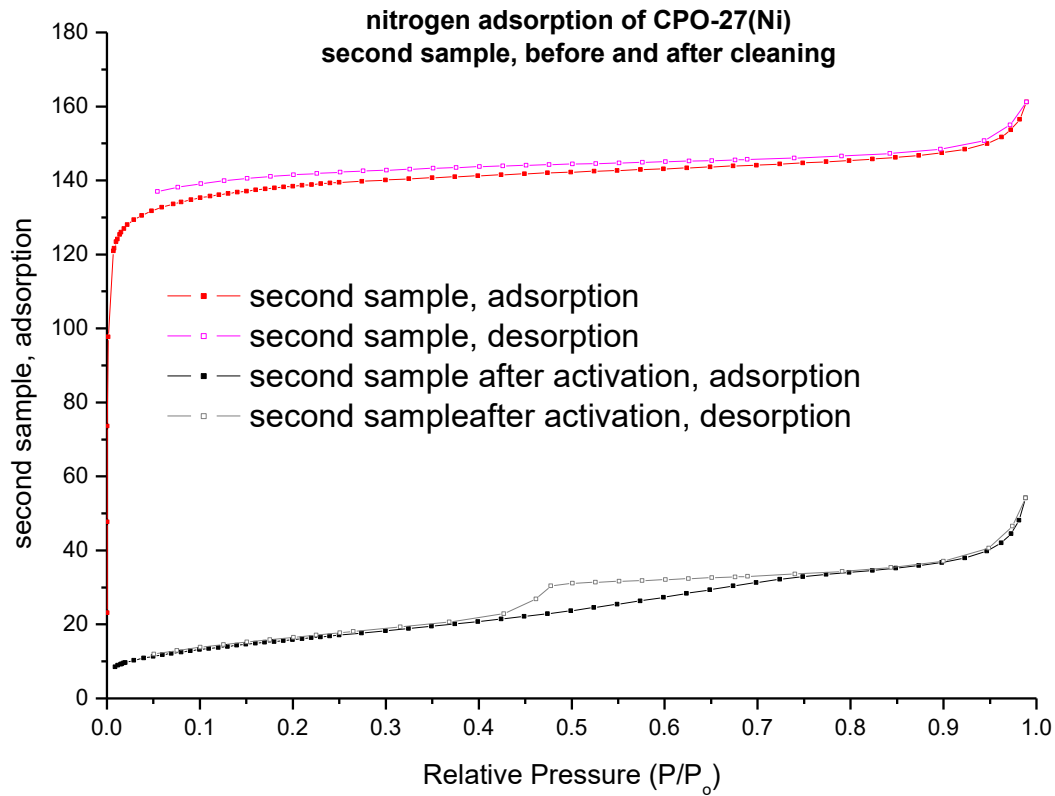
temperatures reach 300°C ^[13], this seems to indicate that the temperature of the MOF has increased to more than what was planned, which likely happened during the vacuum drying, where the sample was placed too close to the heat source (in the bottom). For this reason, a new sample has been synthesized using the same reaction conditions, but the sample was made sure to not touch the bottom with every activation.

It can still be seen from **Graph 30** that the CPO-27(Ni) is highly hydrophilic, with the water adsorption starting at a value of P/P_0 which is very low. This is in accordance to the literature.^[11]



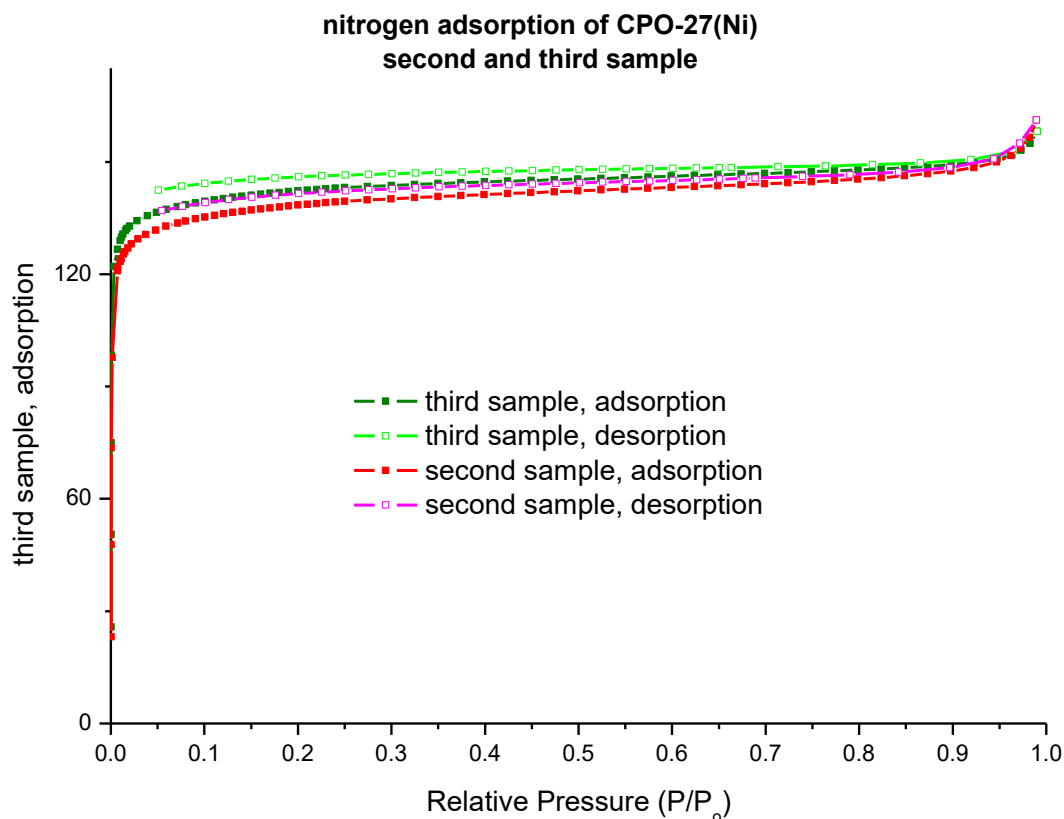
Graph 32 nitrogen adsorption of the first (blue for adsorption and cyan for desorption) and second sample (red for adsorption and magenta for desorption) of CPO-27(Ni).

From the plot as seen in **Graph 32**, the nitrogen adsorption isotherm seems to consist of micropores, which is to be expected from CPO-27(Ni), but the adsorption still seems low as compared to the literature results^[14]. As a result, the sample was activated another time, but this time under a temperature of 250°C using the highest temperature recorded for activation of this MOF. This was kept overnight, followed by a slow cooling under vacuum to prevent oxidation. What was first noticed was the colour change from bright yellow to ochre-brown. Of this sample, a nitrogen adsorption isotherm was performed, which can be seen in **Graph 33**.



Graph 33 nitrogen adsorption of the second sample, before (red for adsorption and magenta for desorption) and after (black for adsorption and grey for desorption) additional activation

It can be seen that the sample has completely lost its structure, which indicates that the activation step at 250°C was too high of a temperature, although the temperature of decomposition is around 400°C in an environment deprived of oxygen^[15]. The decomposition of the structure could indicate that the vacuum is not high enough, since the vacuum oven that has been used operates at a pressure of approximately 50 mbar. For this reason, another vacuum oven (operating at $P < 1$ torr) was used exclusively at 150°C, making sure not to place the samples too close to the bottom. **Graph 34** shows the result of this third sample, as compared to the previous sample, before the additional activation.



Graph 34 nitrogen adsorption of CPO-27(Ni), second sample before activation (red is for adsorption and magenta is for desorption) and third sample (dark green is for adsorption and light green is for desorption)

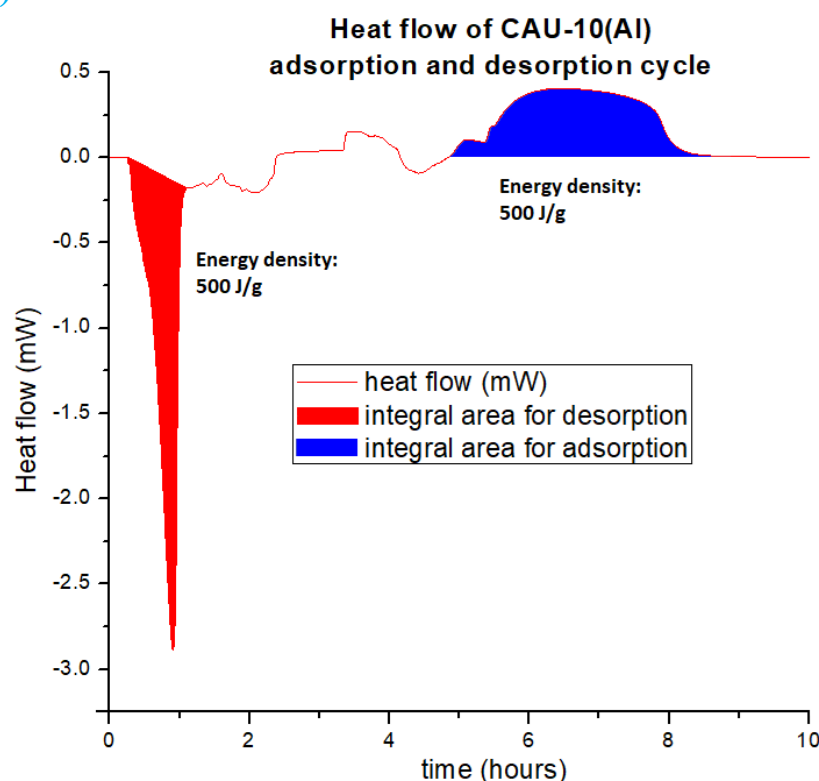
Given the similarities of the isotherms between the samples and the consistently low adsorption, it was therefore initially hypothesized that this is due to water adsorption during the loading of the sample into the nitrogen sorption analyser, causing the adsorbed water to remain on the sample while the nitrogen was being adsorbed. This should not influence the energy density measurement, as all water would first be adsorbed before measuring

6

Energy density

For the energy density, the SENSYS evo TG-DSC-EGA was used. For every sample, 6 mg was weighed in an alumina sample holder, which was placed in the loading position, along with an empty sample holder for reference. The humidity was set at 10 mbar (equal to a relative humidity of 32% at room temperature). This was then initially kept at room temperature for five hours to assure full hydration. Afterwards, the sample was heated at a rate of 10°C/min until 150°C. The profile of the set temperature over time can be seen in **Graph S - 8**. In comparison, the average annual usage of natural gas was used as a reference, multiplied with the Lower Heating Value (LHV) of the gas. The LHV was chosen, since it's in accordance to the European regulations for calculating heating values for natural gas^[16] From this, the needed storage volume of the MOF can be calculated.

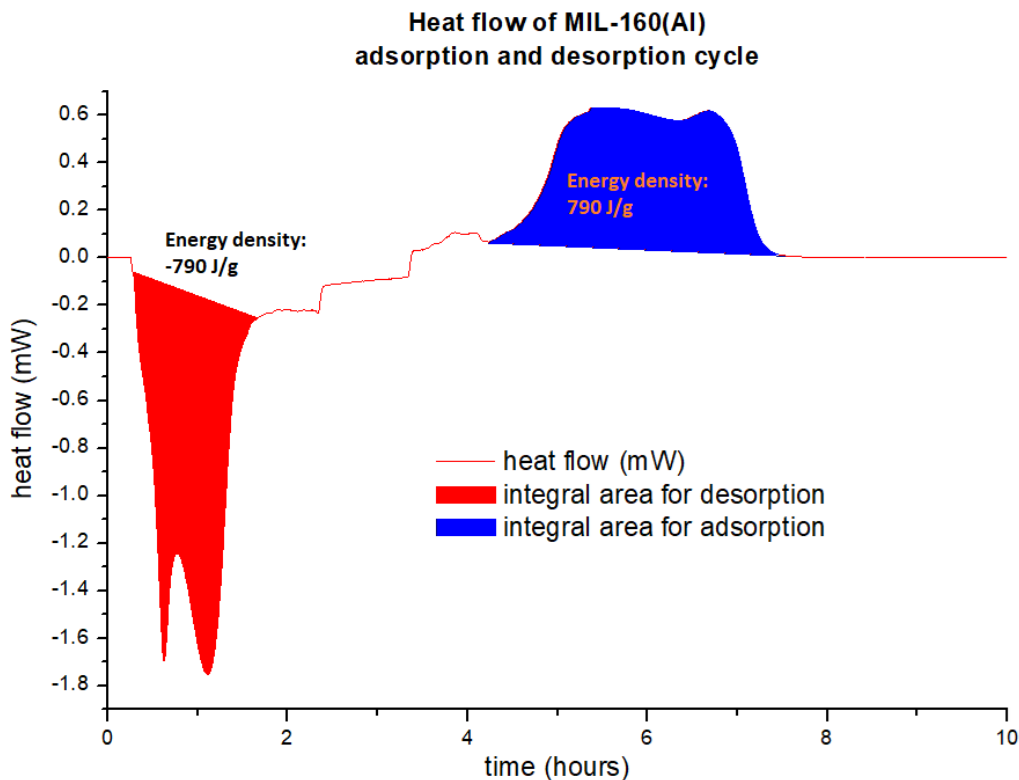
6.1. CAU-10(Al)



Graph 35 plot of the heat flow over the time of the STA measurement of CAU-10(Al), the energy density calculated integrated area of the desorption step is marked red, while the integrated area for the adsorption step is marked blue

From the data as seen in **Graph 35**, it can be seen that the energy density is around 500 J/g. The fact that both integral areas are the same, indicates that the sample was fully dehydrated and hydrated at these intervals.

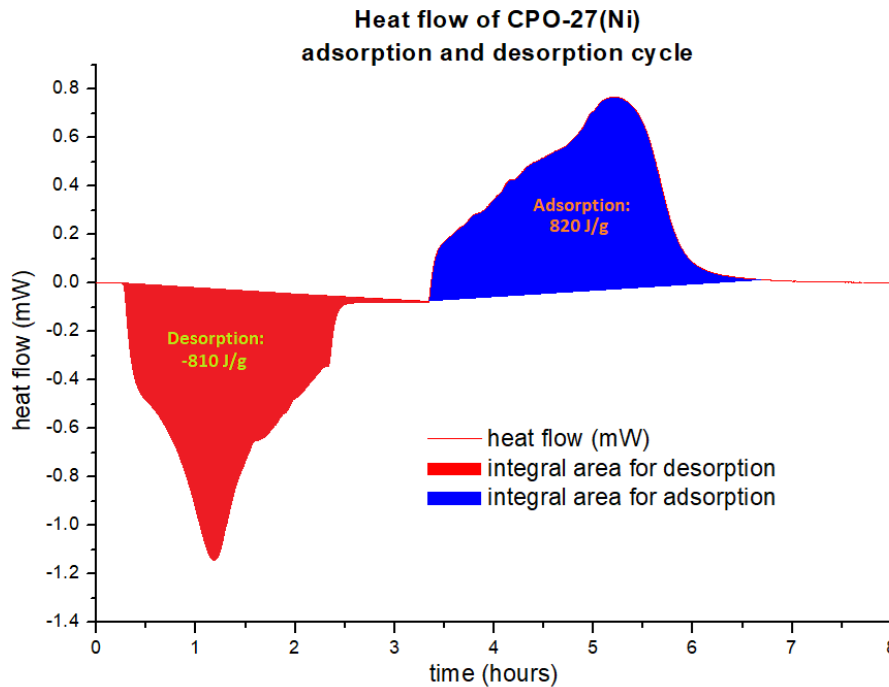
6.2. MIL-160(Al)



Graph 36 Plot of the heat flow over the time of the STA measurement of MIL-160(Al), the integrated area of the desorption step is marked red, while the integrated area for the adsorption step is marked blue

With the weight of the sample of MIL-160(Al) being 6 mg, it was calculated that the energy density was found to be around 790 J/g, from **Graph 36**. The fact that both samples are of the same weight, indicates that all water has been adsorbed and desorbed in the measured intervals. It can be seen that the energy density of MIL-160(Al) is much larger than that of CAU-10(Al), which is likely mostly due to the larger amount of water adsorbed (as seen in **Graph S - 9** and **Graph S - 10**).

6.3. CPO-27(Ni)



Graph 37 Plot of the heat flow over the time of the STA measurement of MIL-160(Al), the integrated area of the desorption step is marked red, while the integrated area for the adsorption step is marked blue

From **Graph 37** it can be seen that the energy density is larger than that of the other two MOFs, but the water adsorption capacity (as seen in **Graph S - 11**) is significantly smaller than that according to the TGA (**Graph 13**) measurements of the sample, where it seems that approximately 52 grams of water can be stored per gram of MOF, which would translate to a water capacity of 34 w/w% , meaning the expected difference in mass would be around -2,1 g , and not -1,3 g. Because the sample has only been pretreated in 150°C, the only explanation can be derived from Dietzel et al.^[17] , where they have found that CPO-27(Ni)'s crystal structure decomposes around 140-190°C. Although they have stated this findings had taken place in air, the use of the vacuum as opposed to oven as opposed to a Schlenck Line can explain the difference between my findings and that of the other literature, since the vacuum used in the literature was at $P < 10^{-5}$ mbar, in a nitrogen environment^[10] , while the activation of this sample took place at $P < 1$ mbar, under a low pressure air environment. This could also explain the lower nitrogen adsorption, although it seems that the adsorption isotherm did not form any mesoporous behaviour, like that what can be seen in **Graph 31**.

Because residential solar heat panels exist that operate under 150°C^[18] , the measured values were taken as the energy density values for this MOF.

6.4. Calculation of the needed storage volume

Assuming a typical Dutch household produces all of the heat from natural gas, the average heat consumption can then be calculated from the annual gas consumption: 1600 m³^[19]. The LHV of the natural gas in the Netherlands is equal to 31,65 MJ/m³^[20]. This means the energy consumption is approximately equal to 51 GJ/year. From this, the needed storage volume can be calculated for the three MOFs:

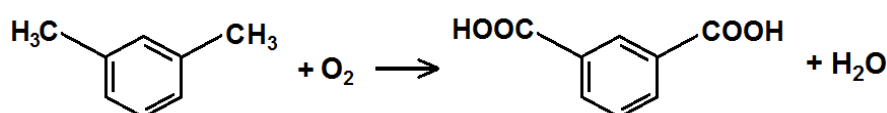
- For CAU-10(Al), the needed amount is equal to 101.000 kg (101 metric tonnes). With a mass density of the MOF being 1,15 g/cm³^[21], the needed volume would be 88 m³.
- For MIL-160(Al), the needed amount is equal to 64.000 kg (64 metric tonnes). With a mass density of 1,0971 g/cm³^[21], this means the volume would be 58 m³.
- For CPO-27(Ni), assuming the loading amount to be the correct amount, the needed storage is equal to 62.000 kg (62 metric tonnes). With the mass density being 1,194 g/cm³^[22], the needed volume becomes 52 m³.

7

Production of the organic linkers

7.1. Isophthalic acid (CAU-10(AI))

Although the production of isophthalic acid from biomass has been under investigation, the only possibility to mass-produce the organic linker is through the oxidation of meta-xylene, using a cobalt-manganese catalyst:



Meta-xylene can be found naturally in tar and petroleum oil^[23]. Although this would make isophthalic acid cheap, a sustainable production of this linker would prove challenging.

7.2. Furandicarboxylic acid (MIL-160(AI))

Although no mass production of the linker has been established to date, the organic substance can be synthesized fully from biomass relatively easily from secondary, lignocellulosic biomass^[23].

Because the chemical structure is similar to terephthalic acid, furandicarboxylic acid is a potential building block in plastics similar to PET plastic, otherwise known as PEF (PolyEthylene Furanoate) plastic. Avantium is the first corporation to mass produce Furandicarboxylic acid from sugars and using this to synthesize PEF bottles^[24]. An economical model has concluded that when PEF plastic would be mass produced, the price could potentially compete with the production of PET plastic^[25].

7.3. 2,5-dihydroxyterephthalic acid (CPO-27(Ni))

No mass-produced synthesis of 2,5-dihydroxyterephthalic acid exists to date, but a synthesis using hydroquinone has been investigated, where its production was successfully performed in a high yield^[10]. Hydroquinone is usually made by reacting aniline in a complex reaction into para-hydroquinone. This can then react in an acidic environment into hydroquinone^[26].

Another way to produce hydroquinone is through quinic acid, which can be found in cinchona bark or coffee beans^[27]. This would enable one to produce the linker entirely from biomass, but this is still just in its research state.

8

Discussion

With the data provided, CPO-27(Ni) seems to have the biggest water adsorption capacity and the highest energy density, but the extremely high hydrophilic properties of this MOF makes them unsuitable for use in this setting, since the MOF would only desorb at a relative humidity of approximately 5%, which is an environment that would likely be too energy consuming for the condenser to achieve. Apart from that, the nickel needed to produce the MOF could prove a challenge when disposing the thermal storage agent for mass-production, since nickel is a polluting agent.

Though CAU-10(Al) seems to have the lowest water adsorption of the three MOFs tested, the high thermal stability of CAU-10(Al) would make this MOF a reliable adsorbent. Another challenge would be the production of this MOF, since research is needed to enable a sustainable production of this MOF. Currently, most isophthalic acid is made from meta-xylene, of which South Korea is the main supplier to date^[27]. The aluminium metal used is however a relatively abundant element, and is less polluting than nickel. MIL-160(Al) appears to have a similar adsorption as CPO-27(Ni), but MIL-160(Al) is thermally more stable and requires less high of a temperature to activate completely. Furandicarboxylic acid is also the easiest to produce among the three linkers of the tested MOFs.

The biggest point of improvement would be to see if CPO-27(Ni) would perform better in a less warm environment, or if an oxygen free environment would increase the thermal stability of CPO-27(Ni). A cooling system could be implemented to prevent the thermal degradation of the MOF.

Another, more minor point for improvement would be that the water adsorption would preferably be performed at a higher precision. The MicroMetetics Tristar II would have been a good solution, but due to time constraints it was chosen to keep the data as is, since the likelihood of this higher precision having an influence on the overall conclusion is unlikely, but having a higher precision would make this MOF

9

Conclusion and recommendations

Although CPO-27(Ni) seems to potentially have the highest adsorption capacity, MIL-160(Al) is thermally more stable, with an adsorption that's similar to CPO-27(Ni). Combined with the fact that it's relatively the easiest way to produce from biomass of the three tested MOFs, makes this the most viable MOF to be used for seasonal thermal energy storage among the MOFs measured. It is therefore assumed that this would apply to all of the eight initial modelled MOFs, and therefore the conclusion is that MIL-160(Al) is the most viable MOF in the use of seasonal thermal energy storage.

Due to its high thermal stability, finding a synthesis method for CAU-10(Al) without the use of DMF could perhaps increase the potential of using this MOF for water adsorption purposes, but this would also mean that a way to produce isophthalic acid from biomass, since this linker is mostly produced by catalytic oxidation of meta-xylene.

If CPO-27(Ni) could somehow be made more thermally stable, this MOF could potentially be used as well, although the highly hydrophilic properties would still pose a challenge to be overcome before it would outperform MIL-160(Al).

Other MOFs, like MOF-841(Zr) or aluminium fumarate would be other options that could be tested in future research. MOF-841(Zr) does seem to have a higher water adsorption, but due to its complexity to synthesize and the unavailability of the linker (meaning this linker must be synthesized before synthesizing the MOF), it was initially not chosen to have this MOF tested for performance. Aluminium fumarate might seem to have a lower adsorption, but the simplicity to produce fumarate from even secondary biomass^[28] would make this a MOF with potential to be used.

A recent study^[29] has also discovered and tested Co_2Cl_2 (BTDD), another MOF with a water adsorption capacity around 80% by mass, approximately twice as high as that of MOF-841(Zr) and MIL-160(Al). This MOF has been tested for performance in clean water production for use in deserts as portable water sources, but this MOF seems very interesting for the use in residential heat storage, due to its sheer water adsorption capacity.

Bibliography

- [1] M. F. de Lange, K. J. F. M. Verouden, T. J. H. Vlugt, J. Gascon and F. Kapteijn, Adsorption-Driven Heat Pumps: The Potential of Metal–Organic Frameworks, *Chemical Reviews*, **12205–12250**, 115 (2015)
- [2] N. May, Eco-balance of a Solar Electricity Transmission from North Africa to Europe, *Diploma thesis*
- [3] <http://comtes-storage.eu/home/seasonal-heat-storage/>, last visited July 31, 2017
- [4] M.S. Godschalk, G. Bakema, 20,000 ATEs systems in the Netherlands in 2020 - major step towards a sustainable energy supply, *a study done for IF Technology*
- [5] <http://energystorage.org/compressed-air-energy-storage-caes>, last visited: July 4th 2017
- [6] M. Linder, C. Roßkopf, M. Schmidt, A. Wörner, Thermochemical Energy Storage in kW-scale based on CaO/Ca(OH)₂, Elsevier, 49, **888–897** (2014)
- [7] M. Polanyi, The Potential Theory of Adsorption, *Science*, 141, **1010–1013** (1963)
- [8] M. F. de Lange, T. Zeng, T. J. H. Vlugt, J. Gascon and F. Kapteijn, Manufacture of dense CAU-10-H coatings for application in adsorption driven heat pumps: optimization and characterization, *Royal Society of Chemistry*, **5911–5920**, 17 (2015)
- [9] A. Cadiou, J. S. Lee, D. D. Borges, P. Fabry, T. Devic, M. T. Wharmby, C. Martineau, D. Foucher, F. Taulelle, C.-H. Jun, Y. K. Hwang, N. Stock, M. F. de Lange, F. Kapteijn, J. Gascon, G. Maurin, J.-S. Chang and C. Serre Metal Organic Framework: Design of Hydrophilic Metal Organic Framework Water Adsorbents for Heat Reallocation, *Advanced Materials*, **32**, **4775–4780**, (2015)
- [10] S. Cadot, L. Veyre, D. Luneau, D. Farrusseng and E. A. Quadrelli, A water-based and high space-time yield synthetic route to MOF Ni₂(dhtp) and its linker 2,5-dihydroxyterephthalic acid, *Journal of Materials Chemistry A*, **17757–17763**, 2, (2014)
- [11] D. Cattaneo, S. J. Warrender, M. J. Duncan, C. J. Kelsall, M. K. Doherty, P. D. Whitfield, I. L. Megson and R. E. Morris, Tuning the nitric oxide release from CPO-27 MOFs, *Royal Society of Chemistry*, **6**, **14059–14067** (2016)
- [12] H. Reinsch, S. Waitschat and N. Stock, Mixed-linker MOFs with CAU-10 structure: synthesis and gas sorption characteristics, *Dalton Transactions*, **42**, **4840–4847** (2013)
- [13] M. Mukoyoshi, H. Kobayashi, K. K. , M. Hayashi, T. Yamada, M. Maesato, J. M. Taylor, Y. Kubota, K. K., M. Takata, T. Yamamoto, S. Matsumura and H. Kitagawa, Hybrid materials of Ni NP@MOF prepared by a simple synthetic method, *Chemical Communications*, **15**, **12463–12466** (2015)
- [14] X. Wu, Z. Bao, B. Yuan, J. Wang, Y. Sun, H. Luo, S. Deng, Microwave synthesis and characterization of MOF-74 (M = Ni, Mg) for gas separation, *Elsevier*, **180**, **114–122** (2013)
- [15] J. Huabc, T. Sun, X. Liu, Y. Guo and S. Wang, Separation of CH₄/N₂ mixtures in metal–organic frameworks with 1D micro-channels, *RSC Advances*, **6**, **64039–64046** (2016)
- [16] <http://eur-lex.europa.eu/legal-content/EN/TXT/?uri=celex%3A32014R0133>, last visited July 31st, 2017
- [17] Pascal D. C. Dietzel, Barbara Panella, Michael Hirscher, Richard Blom and Helmer Fjellvåg, Hydrogen adsorption in a nickel based coordination polymer with open metal sites in the cylindrical cavities of the desolvated framework, *Chemical Communication*, **959–961** (2006)
- [18] Solar Heating and Cooling for Residential Applications, Technology Brief R12 from Energy Technology Systems Analysis Programme and International Renewable Energy Agency (January 2015)
- [19] <https://www.vtwonen.nl/inspiratie/duurzaam-wonen/gemiddeld-gasverbruik/>, last visited July 31st, 2017
- [20] <https://www.energieleveranciers.nl/energie/begrippen/calorische-waarde>, last visited July 31st, 2017
- [21] Daiane Damasceno Borges, Guillaume Maurin, and Douglas S. Galvão, Design of Porous Metal-Organic Frameworks for Adsorption Driven Thermal Batteries, *JACS*, 136(11), **4369–4381** (2014)
- [22] Edder J. García, John P. S. Mowat, Paul A. Wright, Javier Perez-Pellitero, Christian Jallut, and Gerhard D. Pirngruber, Role of Structure and Chemistry in Controlling Separations of CO₂/CH₄ and CO₂/CH₄/CO Mixtures over Honeycomb MOFs with Coordinatively Unsaturated Metal Sites

- [23] R. J. Sheehan, Terephthalic Acid, Dimethyl Terephthalate, and Isophthalic Acid, [Ullmann's Encyclopedia of Industrial Chemistry \(2011\)](#)
- [24] J. Zhang, J. Li, Y. Tang, L. Lin, M. Long, Advances in catalytic production of bio-based polyester monomer 2,5-furandicarboxylic acid derived from lignocellulosic biomass, [Elsevier](#), **130**, **420**, **428** (2015)
- [25] E. de Jong, M. A. Dam, L. Sipos, G.-J. M. Gruter, Furandicarboxylic Acid (FDCA), A Versatile Building Block for a Very Interesting Class of Polyesters, Biobased Monomers, Polymers, and Materials, **1-13** (2012)
- [26] <http://www.lookchem.com/Chempedia/Chemical-Technology/Organic-Chemical-Technology/7762.html>, last visited 4th of July 2017
- [27] Assoah, B., Veiros, L. F., Afonso, C. A. M. and Candeias, N. R., Biomass-Based and Oxidant-Free Preparation of Hydroquinone from Quinic Acid, *Eur. J. Org. Chem.*, **3856-3861** (2016) [21] <http://pulsenews.co.kr/view.php?year=2017&no=315343>, Lotte Chemical to invest \$3.2mn to beef up meta-xylene and polycarbonate production, article last visited on July 4th, 2017
- [28] A. Jiménez-Quero, E. Pollet, M. Zhao, E. Marchioni, L. Avérous, V. Phalip, Itaconic and Fumaric Acid Production from Biomass Hydrolysates by *Aspergillus* Strains, *J. Microbiol. Biotechnol.*, **26(9)**, **1557-1565** (2016)
- [29] A. J. Rieth, S. Yang, E. N. Wang and M. Dincă, Record Atmospheric Fresh Water Capture and Heat Transfer with a Material Operating at the Water Uptake Reversibility Limit, *ACS Central Science* **3(6)**, **668-672** (2017)

Appendix

A.2 Synthesis tables

CAU-10(Al)	mass product				comments
	Al ₂ (SO ₄) ₃	isophthalic acid	(dehydrated)	yield (%)	
premixed	635,7	157,6	371,0	97	- mixed together
predissolved	541,8	159,4			after full characterisation
upscaled 4x (40 mL autoclave)	2559,7	637,7	546,1	71	
upscaled 2x (15 mL autoclave)	1286,5	320,2	108,2	28	
upscaled, sample 1	639,8	160			- mixed together
upscaled, sample 2	639,9	165,9	572,0	98	after IR and XRD
upscaled, sample 3	641,6	158,8			- activated in 250°C

Table S - 1 Collection of all samples of CAU-10(Al) ; the yield is based on the amount of moles of bound linker divided by the amount of moles of isophthalic acid used, the mass of the MOF was based on TGA measurements of the MOF after production, all masses are in mg.

MIL-160(Al)	mass product					comments
	AlCl ₃	fdca	NaOH	(pure, dehydrated)	yield (%)	
first sample	1806,2	1172,9	255,7	321,1	28	
second sample	3620,2	2341,1	606,9	163,1	7,0	- NaOH/fdca = 1,4/1 (mol/mol) ; pH rectified with HCl
third sample	318,2	309,4	115	304,5	96	- NaOH/fdca = 2/1 (mol/mol) ; waited until all dissolved

Table S - 2 Collection of all samples of MIL-160(Al) ; the yield is based on the amount of moles of bound linker divided by the amount moles of furandicarboxylic acid used, the mass of the MOF was based on TGA measurements of the MOF after production, all masses are in mg.

CPO-27	mass product				comments
	Ni(C ₂ H ₅ O ₄) ₂	dhtp	(dehydrated)	yield (%)	
first sample	1253,8	497,5	556,1	84	- placed on bottom of oven
upscaled 4x	5118,5	1996	1894,5	71	- placed on bottom of oven
second sample	1281,4	499	567,6	85	- cleaned with DMF
third sample	1283,4	501,8	578,2	86	

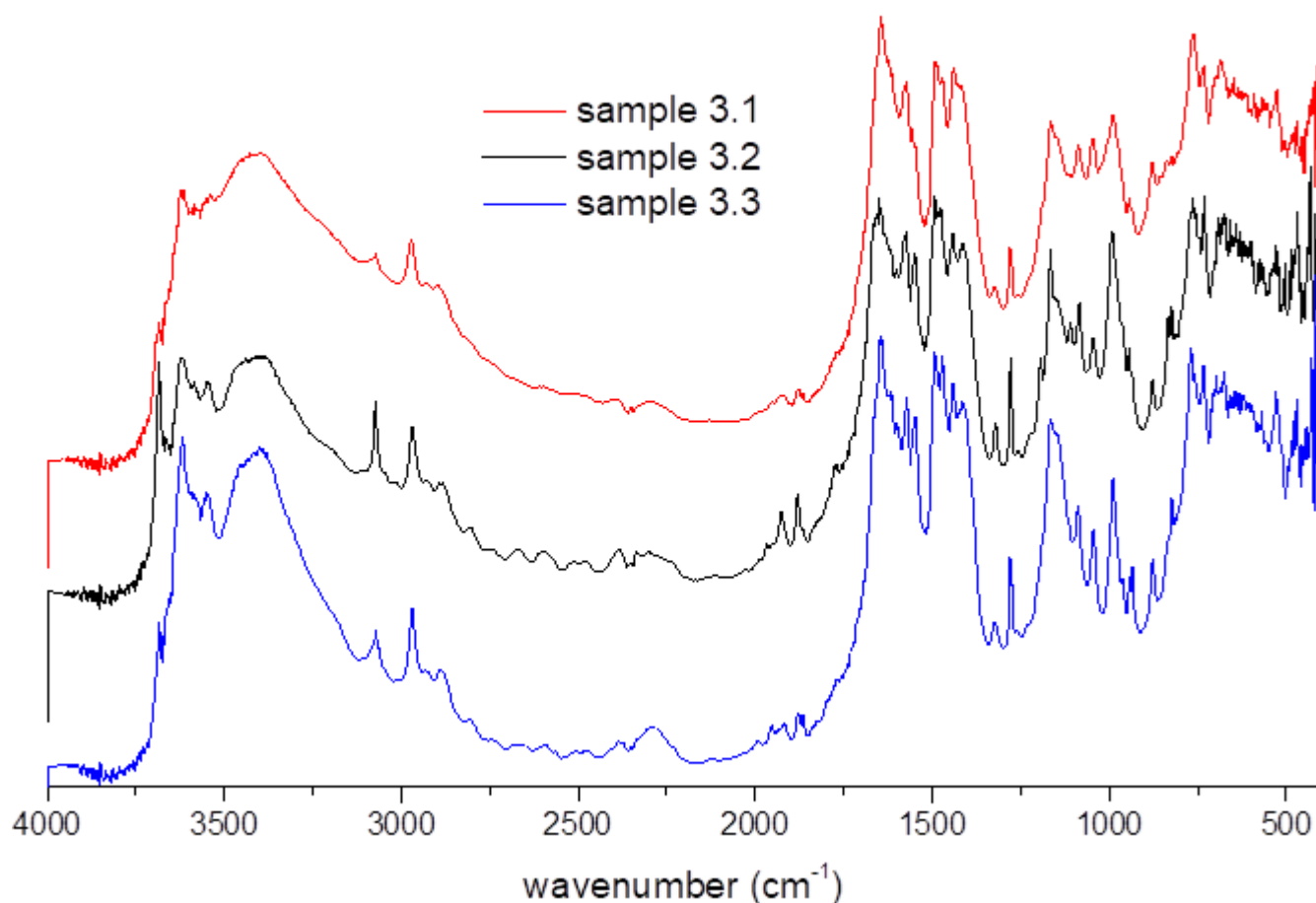
Table S - 3 Collection of all samples of CPO-27(Ni) ; the yield is based on the amount of moles of bound linker divided by the amount of moles of 25-dihydroxyterephthalic acid used, the mass of the MOF was based on TGA measurements of the MOF after production, all masses are in mg.

Here, three tables are presented for all syntheses, one table for each MOF synthesized. The mass given is in mg and the yield calculation was based on the amount of moles of linker bound to the MOF over the amount of organic linker precursor added.

- From a yield perspective, CAU-10(Al) seems to be best synthesized in batches of 150 mg each, as reported in the literature. Increasing the amount of precursor by a factor of 4 and using a 40 mL seems to decrease the yield significantly, while keeping the autoclave volume constant with twice the amount of precursor seems to decrease the yield drastically. It seems that the “fill factor” ($V_{\text{mixture}} / V_{\text{autoclave}}$) is determining, where the amount given in the literature is optimal.
- Synthesizing MIL-160(Al) according to the literature seems to have a fairly low yield. Adding hydrochloric acid not only decreases the yield drastically, but also yields a product contaminated with free unreacted linker. The MOF is best synthesized with twice the amount of sodium hydroxide, while letting the furandicarboxylic acid react with the hydroxide, making a clear solution before adding the aluminium chloride.
- From the synthesis of CPO-27(Ni), it can be seen that upscaling to four times the initial amount, as reported by the literature, this decreases the yield mildly. This could be due to a lower end reaction rate, so the sample would require more time to react than an overnight reaction.

A.2 infrared spectroscopy of the third batch of CAU-10(Al) samples

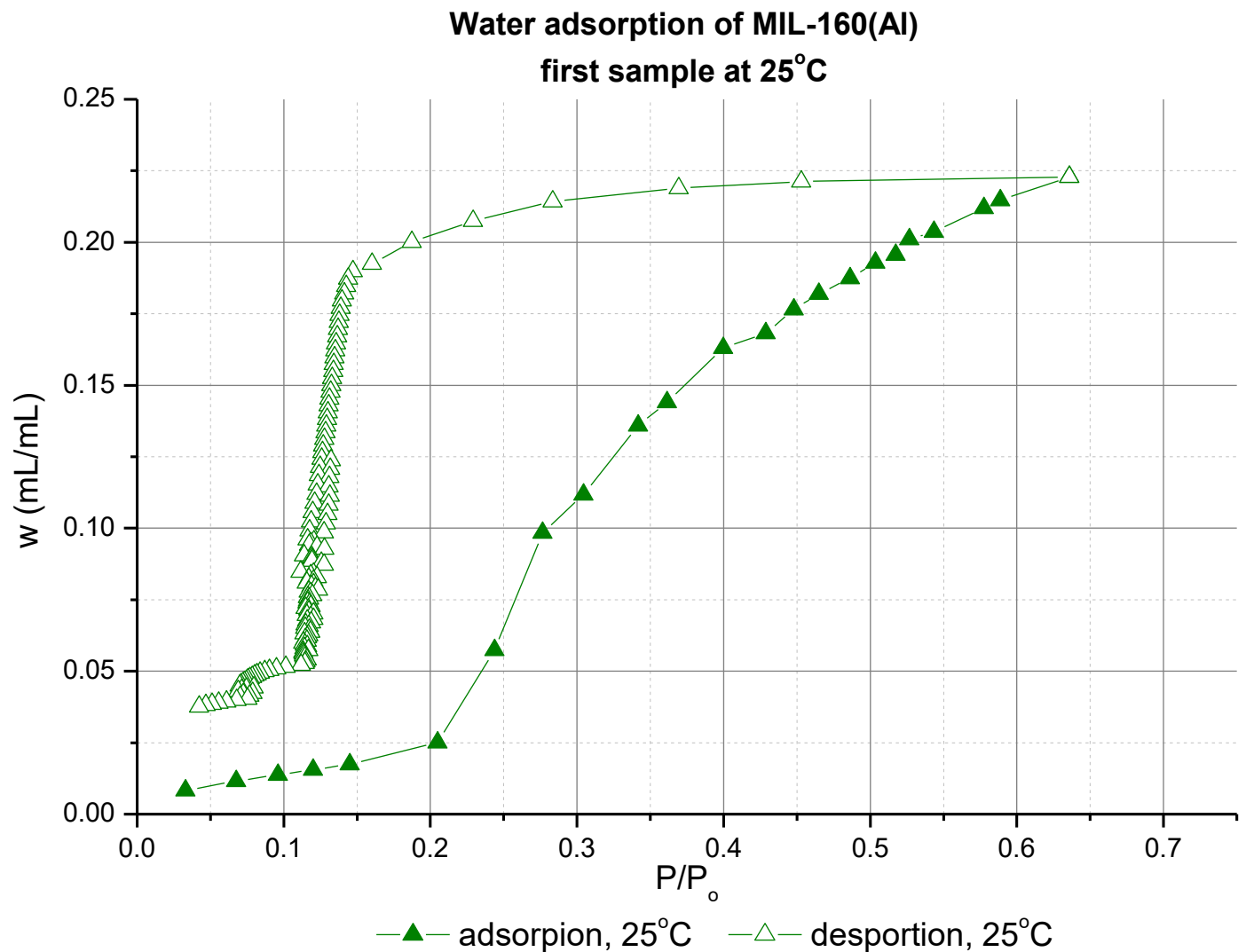
Infrared spectroscopy of the third batch of samples of CAU-10(Al)



Graph S - 1 Infrared spectroscopy of the three new samples of CAU-10(Al), shifted vertically to better show any differences in the peaks

This graph shows the three samples of the third batch of CAU-10(Al), as seen in [Appendix A.2](#). Apart from showing no measurable signs of impurities, the three spectra also showed to be identical, with only a difference in peak ratio being visible. With this data, it was chosen to combine the three samples in one sample holder for pragmatic reasons.

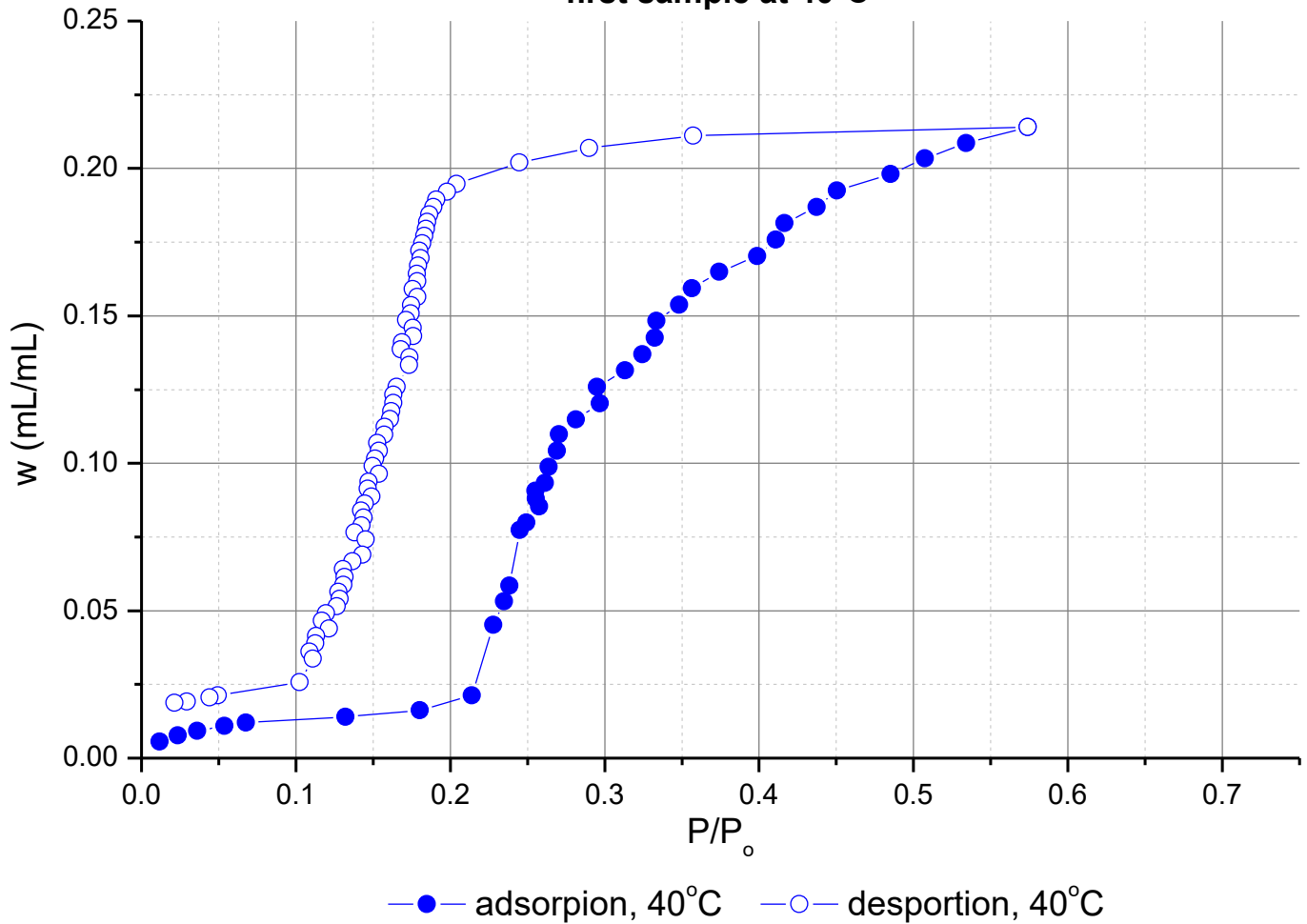
A.3 water adsorption of the first sample of MIL-160(Al)



Graph S - 2 Water adsorption isotherm of the first sample of MIL-160(Al) at 25°C, measured over $0 < P/P_0 < 0,65$, using the Quantachrome Vstar sorption analyzer

This shows the adsorption of the first sample MIL-160(Al) measured under a temperature of 25°C, as seen in **Graph 21**. Likely due to its low adsorption temperature, this isotherm shows a large hysteresis between the adsorption and desorption. The larger amount of measuring points during desorption probably means that the desorption likely is more in accordance to the equilibrium values than the adsorption, since this would mean more time has passed for the desorption to take place.

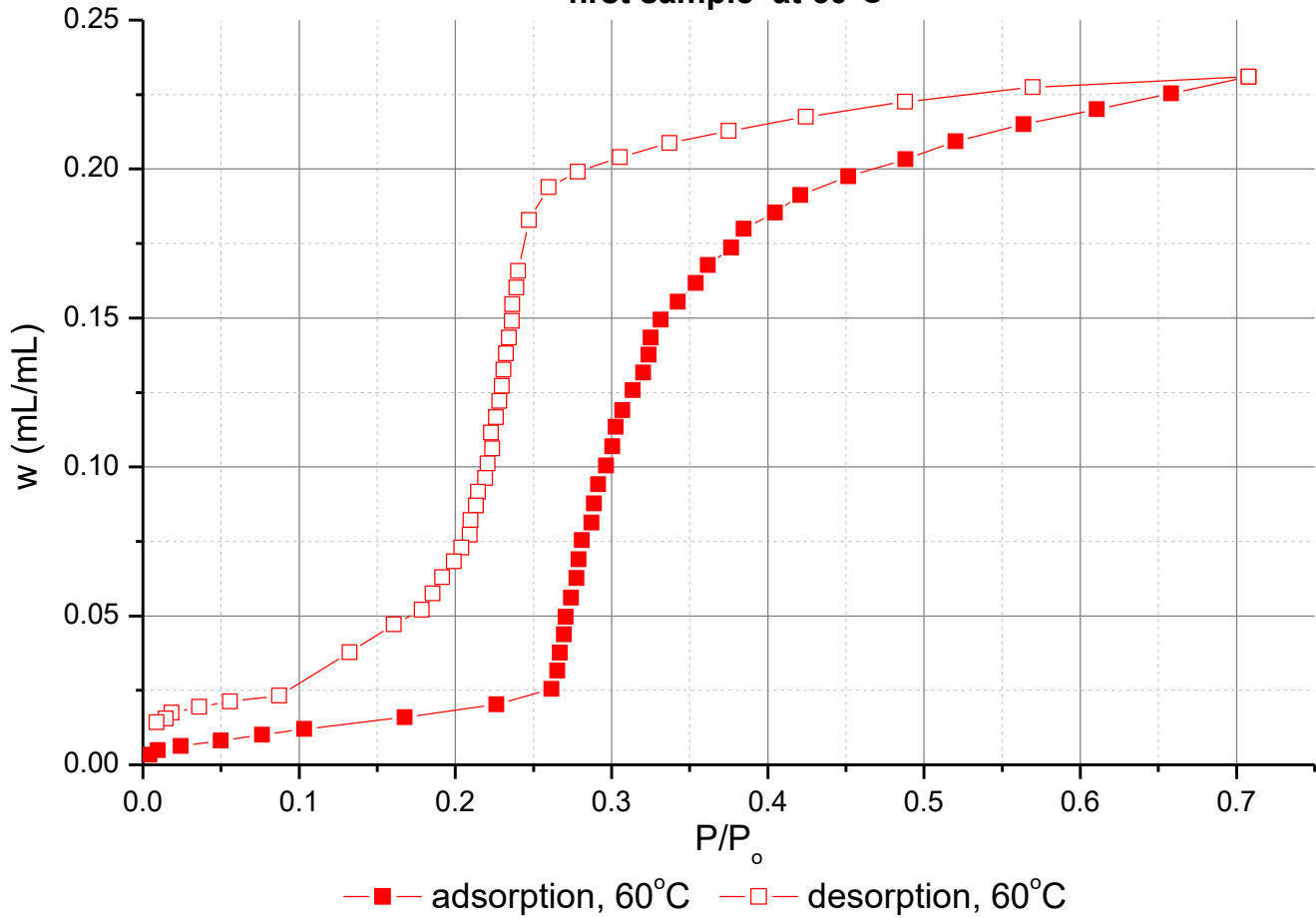
**Water adsorption of MIL-160(Al)
first sample at 40°C**



Graph S - 3 Water adsorption isotherm of the first sample of MIL-160(Al) at 40°C, measured over $0 < P/P_0 < 0,55$, using the Quantachrome Vstar sorption analyzer

This shows the adsorption of the first sample MIL-160(Al) measured under a temperature of 40°C, as seen in [Graph 21](#). Likely due to its low adsorption temperature, this isotherm shows a relatively large hysteresis between the adsorption and desorption. Though more adsorption points were measured in the adsorption as compared to the isotherm measured at 25°C, The larger amount of measuring points during desorption would still make the desorption more likely in accordance to the equilibrium values than the adsorption.

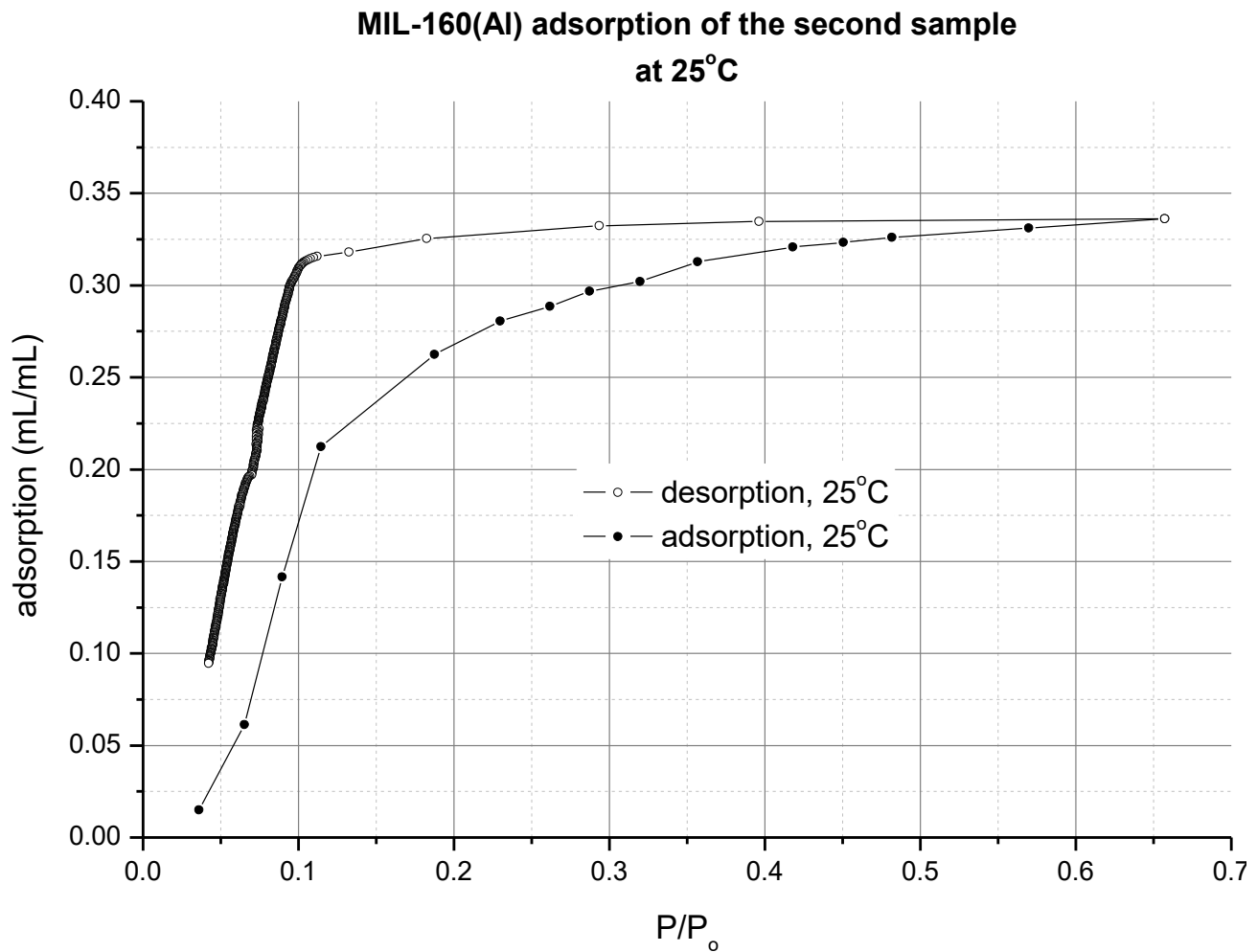
**water adsorption of MIL-160(Al)
first sample at 60°C**



Graph S - 4 Water adsorption isotherm of the first sample of MIL-160(Al) at 60°C, measured over $0 < P/P_0 < 0,7$, using the Quantachrome Vstar sorption analyzer

This shows the adsorption of the first sample MIL-160(Al) measured under a temperature of 60°C, as seen in **Graph 21**. The higher measuring temperature has led to the hysteresis to be smaller, as compared to the isotherms measured at 25 and 40°C. Given that the amount of measurement points during adsorption is about as much as the desorption, both the adsorption and desorption are similar in precision, as compared to the equilibrium values.

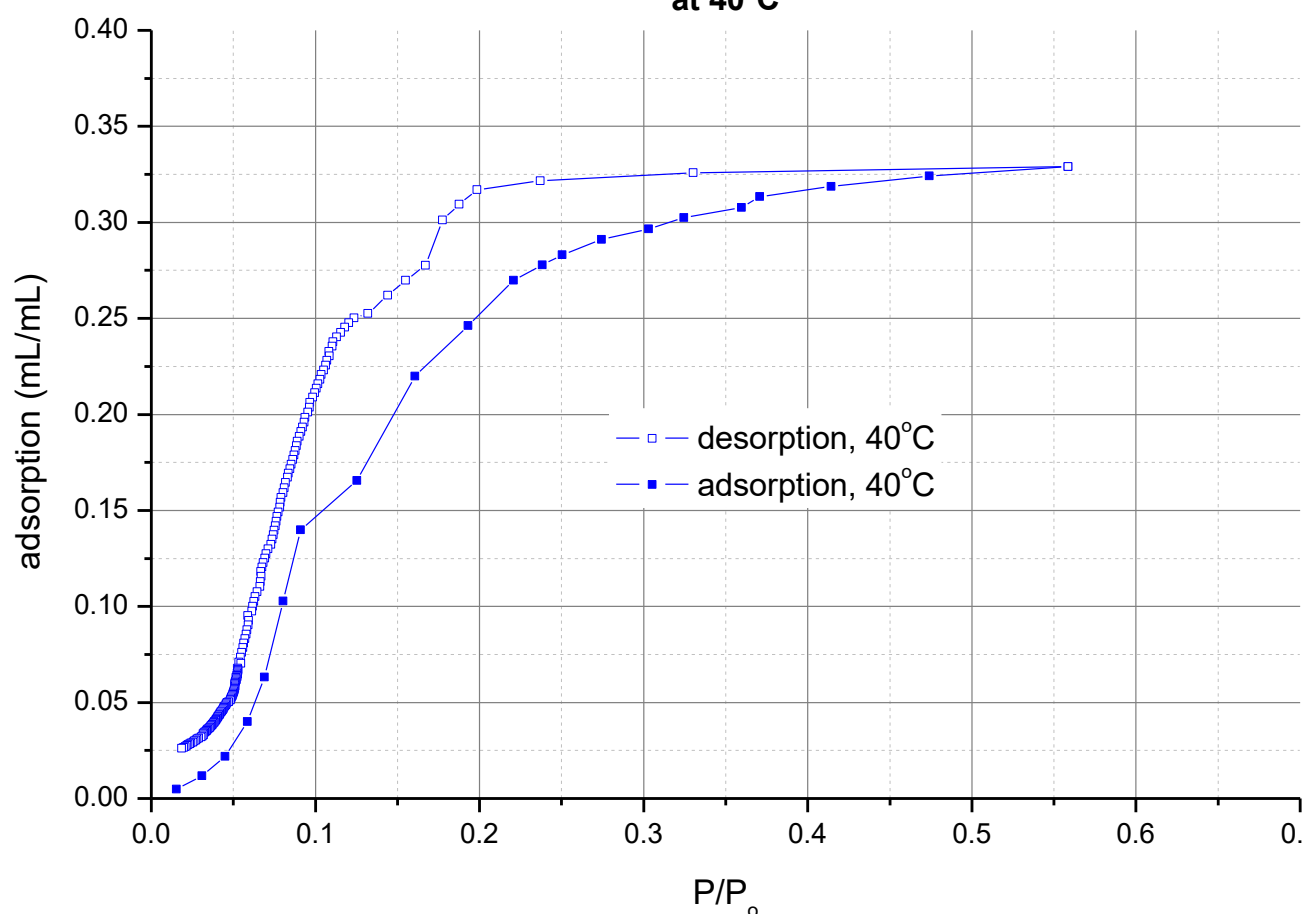
A.4 water adsorption of the second sample of MIL-160(Al)



Graph S - 5 Water adsorption of second sample of MIL-160(Al) under 25°C, measured over $0 < P/P_0 < 0,65$, using the Quantachrome Vstar sorption analyzer

This shows the adsorption of the second sample MIL-160(Al) measured under a temperature of 25°C, as seen in **Graph 28**. The hysteresis seen from this plot is significantly smaller than that of the first sample (as seen in **Graph S - 2**). This indicates that the impurities were the inhibitors of the adsorption, since this indicates that the kinetics were faster. The capacity has increased as well, which can also be explained to the higher purity of the MOF. The larger amount of measuring points during desorption probably means that the desorption likely is more in accordance to the equilibrium values than the adsorption, since this would mean more time has passed for the desorption to take place.

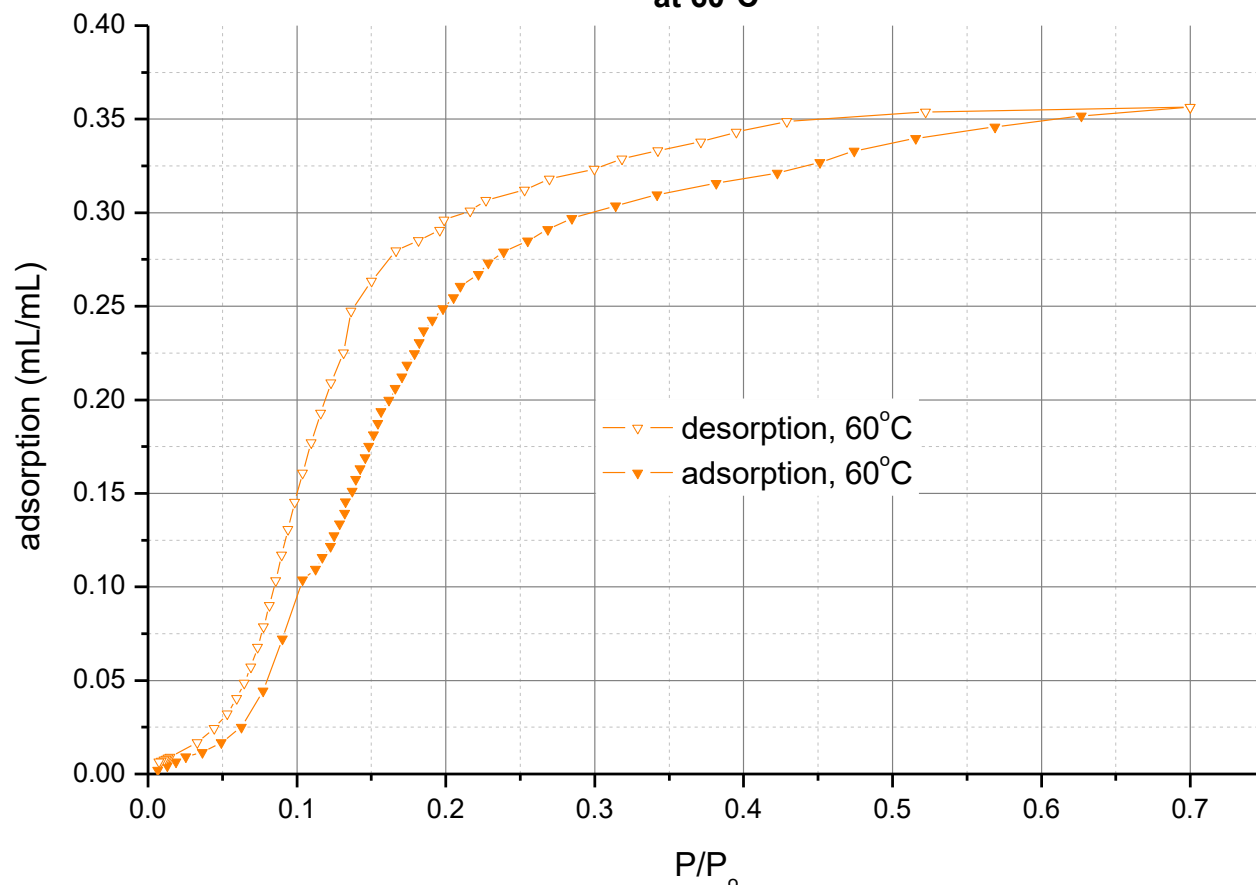
MIL-160(Al) adsorption of the second sample at 40°C



Graph S - 6 Water adsorption of MIL-160(Al) under 40°C, measured over $0 < P/P_0 < 0,55$, using the Quantachrome Vstar sorption analyzer

This shows the adsorption of the second sample MIL-160(Al) measured under a temperature of 40°C, as seen in **Graph 28**. The hysteresis seen from this plot is significantly smaller than that of the first sample (as seen in **Graph S - 3**). This indicates that the impurities were inhibiting the adsorption, since the kinetics seem to be faster. The capacity has increased as well, which can also be explained to the higher purity of the MOF. The larger amount of measuring points during desorption (especially towards the end) probably means that the desorption likely is more in accordance to the equilibrium values than the adsorption, since this would mean more time has passed for the desorption to take place.

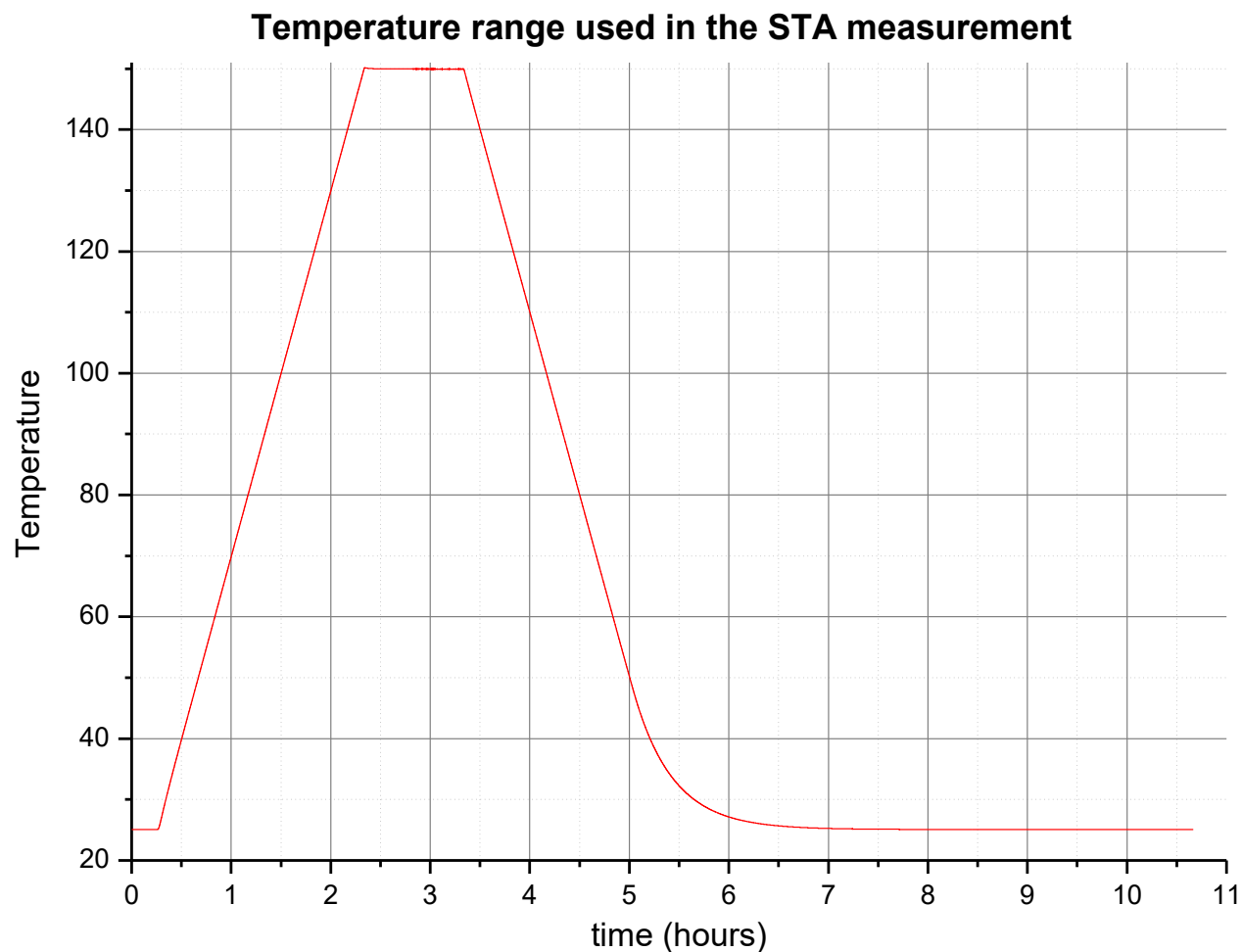
MIL-160(Al) adsorption of the second sample at 60°C



Graph S - 7 Water adsorption of MIL-160(Al) under 60°C, measured over $0 < P/P_0 < 0,7$, using the Quantachrome Vstar sorption analyzer

This shows the adsorption of the second sample MIL-160(Al) measured under a temperature of 60°C, as seen in **Graph 28**. The hysteresis seen from this plot is significantly smaller than that of the first sample (as seen in **Graph S - 4**). This indicates that the impurities were inhibiting the adsorption, since the kinetics seem to be faster. The capacity has increased as well, which can also be explained to the higher purity of the MOF. The indentation at $P/P_0 = 0,1$ can be explained by a difference in measuring settings of the Vstar during measuring.

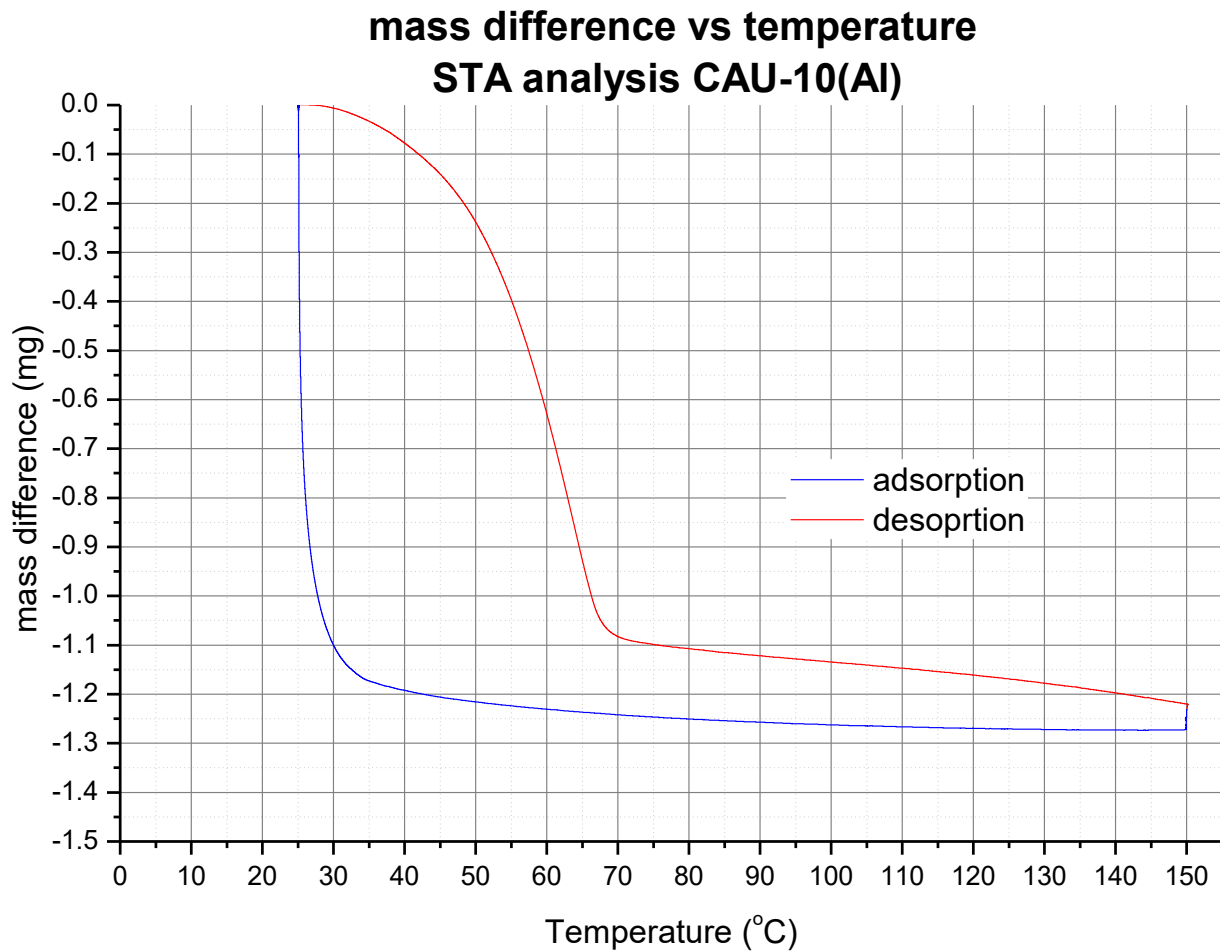
A.5 Temperature profile used for the STA measurements



Graph S - 8 Temperature profile, as set for the Evasys STA measurement. The environment 32% relative humidity. Before $t = 0$, the sample was held at 25°C for 5 hours. Between $t \approx 0,5$ h and $t \approx 2,5$ h, the temperature was increased with a heating rate of 10°C/min, from 25°C to 150°C. this temperature was kept for 1 hour to assure complete dehydration, followed by cooling at a cooling rate of 10°C/min. This temperature was then kept for 5 hours.

This shows the temperature profile used in the STA measurements (**Graph 35**, **Graph 36** and **Graph 37**). The temperature was first set at 25°C for five hours prior to measuring ($t = 0$). This was followed by heating the sample at a rate of 10°C/min until a temperature of 150°C was reached. This temperature was kept for 1 hour, followed by cooling back down to 25°C at a rate of 150°C, and keeping the resulting temperature constant for 5 hours.

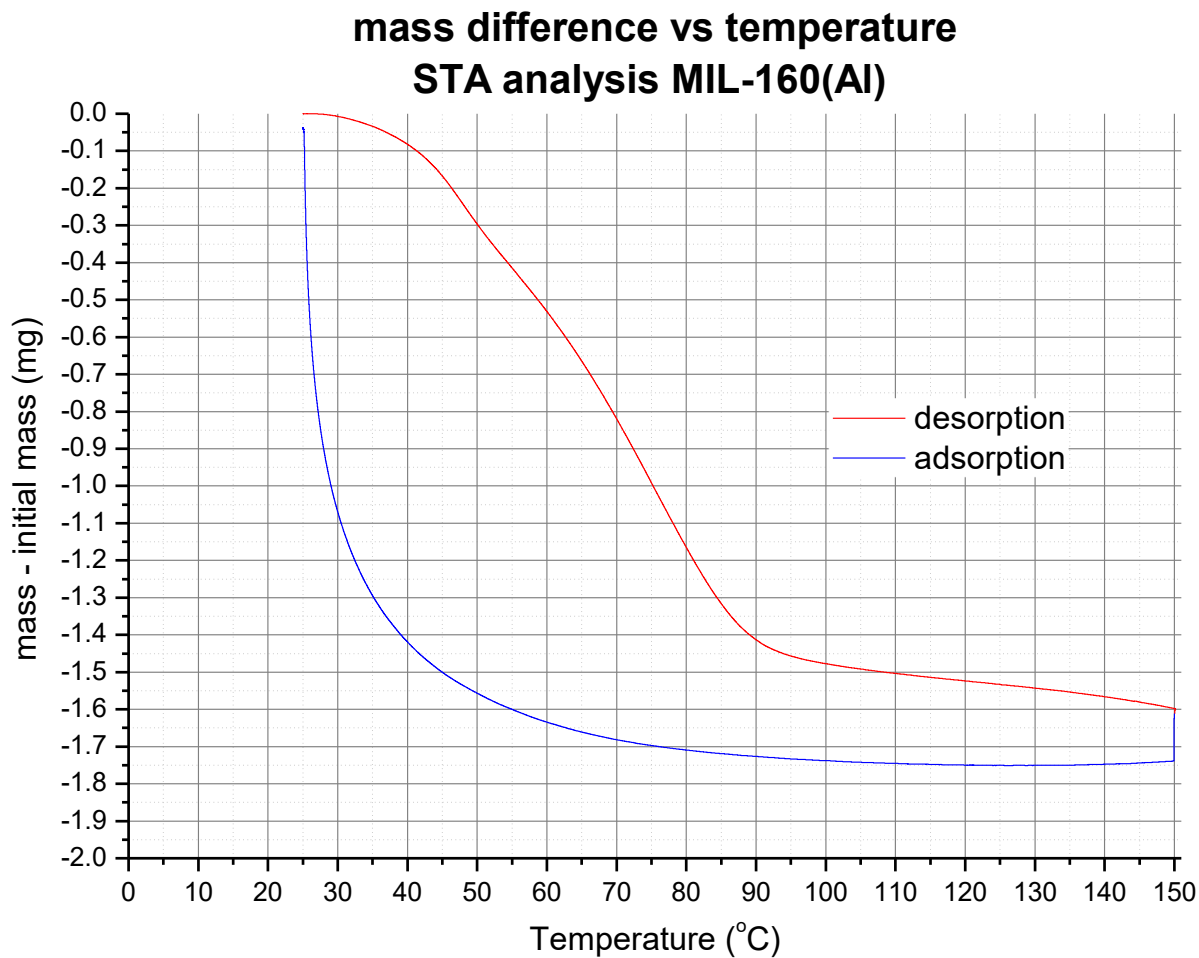
A.6 TGA profile of CAU-10(Al) used for the STA measurements



Graph S - 9 Mass difference (mass – 6 mg, the initially weighed mass) of the CAU-10(Al) sample vs temperature, during the full cycle. The adsorption is blue, while the desorption is in red

This shows the mass difference (as defined by the mass measured minus the initial mass weighed: 6 mg) versus the temperature measured for the CAU-10(Al) sample (**Graph 35**). It can be seen that approximately 1,3 mg was desorbed during the cycle, which is in accordance with the TGA measurements.

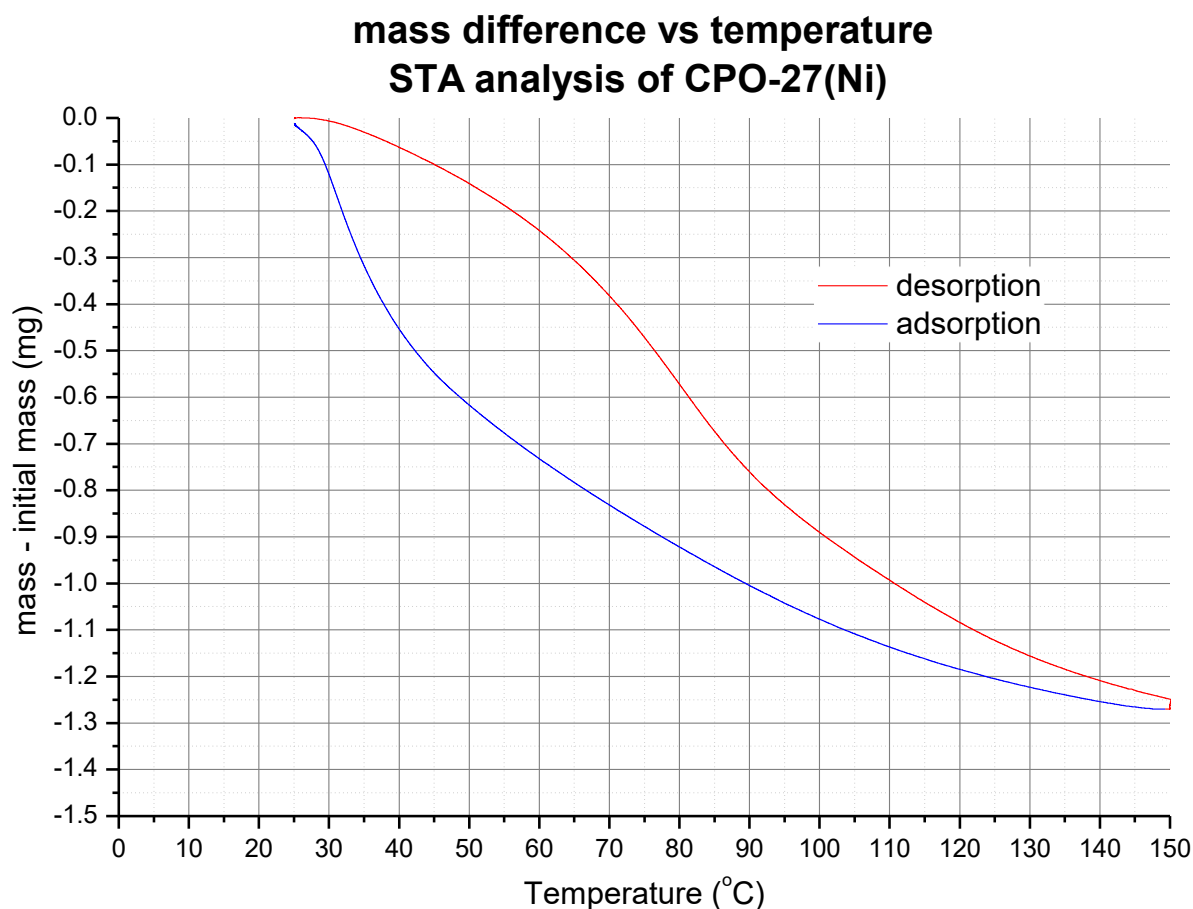
A.7 TGA profile of MIL-160(Al) used for the STA measurements



Graph S - 10 Mass difference (mass – 6 mg, the initially weighed mass) of the MIL-160(Al) sample vs temperature, during the full cycle. The adsorption is blue, while the desorption is in red

This shows the mass difference (as defined by the mass measured minus the initial mass weighed: 6 mg) versus the temperature measured for the MIL-160(Al) sample ([Graph 36](#)). It can be seen that approximately 1,75 mg was desorbed during the cycle, which is in accordance with the TGA measurements.

A.8 TGA profile of CPO-27(Ni) used for the STA measurements



Graph S - 11 Mass difference (mass – 6 mg, the initially weighed mass) of the CPO-27(Ni) sample vs temperature, during the full cycle. The adsorption is blue, while the desorption is in red

This shows the mass difference (as defined by the mass measured minus the initial mass weighed: 6 mg) versus the temperature measured for the CPO-27(Ni) sample ([Graph 37](#)). It can be seen that approximately 1,25 mg was desorbed during the cycle, which is lower as compared to the other TGA measurements. This indicates a degradation of the MOF's structure.